ACS APPLIED BIO MATERIALS

www.acsabm.org Article

Peptide-Conjugated Ultrasmall Gold Nanoparticles (2 nm) for Selective Protein Targeting

Tatjana Ruks, Kateryna Loza, Marc Heggen, Oleg Prymak, Andre Luiz Sehnem, Cristiano L. P. Oliveira, Peter Bayer, Christine Beuck,* and Matthias Epple*

Cite This: *ACS Appl. Bio Mater.* 2021, 4, 945−965 Read Online

ACCESS | Metrics & More | Article Recommendations | Supporting Information

ABSTRACT: Ultrasmall gold nanoparticles with a metallic core diameter of 2 nm were surface-conjugated with peptides that selectively target epitopes on the surface of the WW domain of the model protein hPin1 (hPin1-WW). The binding to the gold surface was accomplished via the thiol group of a terminal cysteine. The particles were analyzed by NMR spectroscopy, high-resolution transmission electron microscopy, and differential centrifugal sedimentation. The surface loading was determined by conjugating a FAM-labeled peptide, followed by UV−vis spectroscopy, and by quantitative ^{1}H NMR spectroscopy, showing about 150 peptide molecules conjugated to each nanoparticle. The interaction between the peptide-decorated nanoparticles with hPin1-WW was probed by ^{1}H−^{15}N-HSQC NMR titration, fluorescence polarization spectroscopy (FP), and isothermal titration calorimetry (ITC). The particles showed a similar binding (K_D = 10−20 μM) compared to the dissolved peptides (K_D = 10−30 μM). Small-angle X-ray scattering (SAXS) showed that the particles were well dispersed and did not agglomerate after the addition of hPin1-WW (no cross-linking by the protein). Each nanoparticle was able to bind about 20 hPin1-WW protein molecules. An unspecific interaction with hPin1 was excluded by the attachment of a nonbinding peptide to the nanoparticle surface. The uptake by cells was studied by confocal laser scanning microscopy. The peptide-functionalized nanoparticles penetrated the cell membrane and were located in the cytosol. In contrast, the dissolved peptide did not cross the cell membrane. Peptide-functionalized nanoparticles are promising agents to target proteins inside cells.

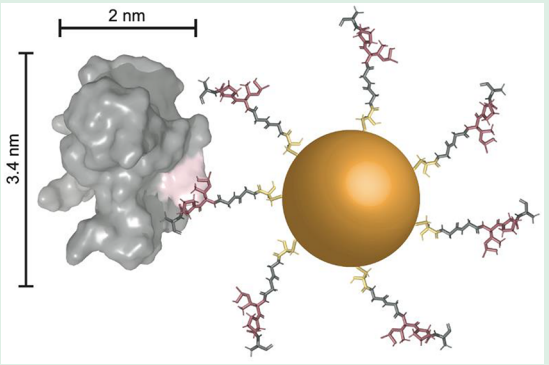

KEYWORDS: *gold nanoparticles, peptides, proteins, supramolecular chemistry*

INTRODUCTION

Supramolecular targeting of proteins by binders is an exciting area of current chemistry. A selective recognition of epitopes on a protein surface opens attractive possibilities to influence their function or conformation. In this regard, a number of molecular protein binders have been developed and tested.[1−4] Like molecular binders, nanoparticles have also shown a high potential for protein targeting.[5−8]

Among nanoparticles, ultrasmall gold nanoparticles with a diameter around 2 nm have a high potential to act as a supramolecular transport system.[9−22] Being at the borderline to atom-precise metal clusters,[23−29] they are smaller than a typical protein and, after a suitable surface functionalization with a specific ligand (usually via a thiol group),[30] they may be used to address epitopes on a protein surface. This requires that the ligand is still effective after it was bound to the gold nanoparticle surface. Peptides are common ligands for gold nanoparticles, but in general, the nanoparticles used are bigger (10 or more nm),[31−42] therefore their interaction with individual proteins is difficult to assess. Furthermore, NMR spectroscopy is not possible with nanoparticles of "standard size" (>10 nm) due to the vicinity of the metallic core,[43−45] i.e. this versatile method to study protein−ligand interactions[46] is not applicable for "standard" nanoparticles.

To study the interaction of specifically surface-functionalized gold nanoparticles with proteins, we used the N-terminal WW domain of the protein human Pin1 (hPin1-WW) as model target system. hPin1 is a cell cycle regulatory proline (P) *cis/trans*-isomerase whose WW domain binds to phosphorylated and proline-rich unstructured peptides and consists of 39 amino acids.[47,48] A phosphothreonine-proline motif (pTP) is a specific binder to hPin1-WW.[49] Therefore, we chose the small hexapeptide CGGpTPA and the 9-mer peptide CGSGGGpTPA as specific binding ligands for the WW domain. Cysteine (C) provided the thiol-group for attachment

Received: November 2, 2020
Accepted: December 23, 2020
Published: January 4, 2021

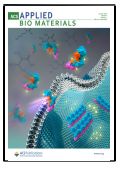

https://dx.doi.org/10.1021/acsabm.0c01424
ACS Appl. Bio Mater. 2021, 4, 945−965

to the gold nanoparticle surface whereas the two glycines (GG) or the longer GSGGG sequence acted as spacer between the binding motif and the gold nanoparticle core. Ultrasmall gold nanoparticles carried this peptide on the surface to specifically target hPin1-WW.

Here, we report a comprehensive proof-of-concept study where peptide-functionalized nanoparticles interact with the model protein hPin1-WW.

EXPERIMENTAL SECTION

Chemicals. An aqueous solution of chloroauric(III) acid sodium salt ($NaAuCl_4$, prepared by dissolving sodium chloroaurate(III) dihydrate ($NaAuCl_4 \cdot 2H_2O$, Sigma-Aldrich; 99%) in hydrochloric acid (37%) and ultrapure water; 0.024 M Au) was used as a gold source. Sodium borohydride ($NaBH_4$, Sigma-Aldrich; ≥96%) in solution was used as a reducing agent. For protein-interaction studies, the gold nanoparticles were coated with the phosphorylated synthetic model peptide CGGpTPA (95−99%) and its derivatives: CGGpTP-(A*-^{15}N)-NH_2 (purity 99%), CGGpTPAAK-5,6-FAM-NH_2 (5,6-FAM = 5,6-carboxyfluorescein; degree of labeling 92−96%), CGSGGGpTPA (98−99%), and CGSGGGTDA (purity 95%; nonbinding model peptide).

All peptides were obtained from Caslo ApS (Denmark) as lyophilized hydrochloride salts. They were used as received without further purification. The gold nanoparticles were stored in potassium phosphate buffer (47 mM K_2HPO_4 and 3 mM KH_2PO_4, pH 8) after the synthesis. In all experiments, ultrapure water with a specific resistivity of 18.2 MΩ (Purelab ultra instrument from ELGA) was used as solvent unless otherwise stated. All glassware was cleaned with boiling *aqua regia* and ultrapure water before all reactions involving nanoparticles.

The formation of peptide disulfides must be minimized during the synthesis (requiring to work under inert gas atmosphere to avoid the oxidation of thiols[50,51]) as we have observed that these disulfides were very difficult to remove from the nanoparticle dispersion after they had formed.

Nanoparticle Synthesis. For the syntheses of peptide-functionalized gold nanoparticles, 1.5−18.8 μmol peptide was dissolved in 2−25 mL degassed water, and the pH was adjusted to 5.5−5.7 with 0.1 M sodium hydroxide solution. The amounts of $NaAuCl_4$ and $NaBH_4$ were adapted according to the molar amount of the peptide. A low pH was necessary to minimize the oxidation of the thiol group to disulfide which does not bind to the nanoparticle and is difficult to remove. However, the pH must not be too low as this would lead to an enhanced decomposition of $NaBH_4$ in the next step. Then, 20.8−263 μL $NaAuCl_4$ (corresponding to 0.5−6.3 μmol gold) was added to the peptide solution under stirring. The peptide/gold mixture rapidly changed from yellow to colorless, indicating that the gold ions were reduced from Au^{+III} to Au^{+I} by oxidation of the thiol groups to disulfide groups. After 10 min of cooling the mixture in an ice bath, 10−126 μL of 0.2 M $NaBH_4$ solution (freshly prepared with 4 °C cold water; corresponding to 2−25.2 μmol $NaBH_4$) was added and stirred for another hour to reduce Au^{+I} to Au^0. All syntheses were carried out under inert gas atmosphere (argon, Schlenk technique).

Purification of the gold nanoparticles was done by ultracentrifugation for 15 h at 30 000 rpm. After that, there were two phases, i.e. the concentrated gold nanoparticle dispersion (dark brown) in the lower part of the centrifugation tube and unreacted starting materials and synthesis byproducts (colorless) in the upper part. The colorless phase was carefully removed with a pipet. The nanoparticle dispersion was purified by spin filtration with an Amicon spin filter (MWCO 3 kDaA, 0.5 mL) for 15 min at 14 000*g*. Then, the nanoparticles were multiply washed with potassium phosphate buffer (50 mM, pH 8) by redispersion/spin filtration. Recovery of the concentrated nanoparticle dispersion was done by centrifugation at 1000*g* for 2 min. The resulting volume of the purified and concentrated nanoparticle dispersion was in the range of 50−60 μL.

For gold nanoparticles conjugated with the fluorescent peptide CGGpTPAAK-5,6-FAM-NH_2, 1.5 μmol of peptide was dissolved in 2 mL degassed water, and the pH was adjusted to 8 with 0.1 M NaOH. A higher pH was necessary to avoid the precipitation of the FAM-labeled peptide during the synthesis. Then, 0.02 mL of $NaAuCl_4$ (0.5 μmol) was added to the peptide solution under stirring. After 10 min of cooling the mixture in an ice bath, 0.01 mL of $NaBH_4$ (2 μmol, freshly dissolved in 4 °C cold water) was added and the mixture was stirred for 1 h. The synthesis was done under inert gas atmosphere. Purification was done by spin filtration with an Amicon spin filter (MWCO 3 kDaA, 2 and 0.5 mL) for 15 min at 14 000*g*. The nanoparticles were washed with potassium phosphate buffer (50 mM, pH 8) until the filtrate was colorless. The resulting volume of concentrated nanoparticle dispersion was in the range of 50−60 μL. Recovery of the concentrated nanoparticle dispersion was accomplished by centrifugation at 1000*g* for 2 min.

Protein Synthesis and Characterization. The ^{15}N-labeled hPin1-WW domain (residues 3−39; hPin1-WW; PDB ID: 2M8I) was expressed as N-terminal GST fusion protein with a PreScission protease cleavage site and purified as described earlier.[46] Briefly, the ^{15}N-labeled protein was expressed in *E. coli* BL21 (DE3) T1r in M9 minimal medium containing $^{15}NH_4Cl$ as sole nitrogen source, while unlabeled protein for ITC and fluorescence anisotropy experiments was expressed in LB medium. The protein was purified by GSH affinity chromatography, the GST tag was cleaved with PreScission protease and the WW domain was isolated by size exclusion chromatography. Protein NMR samples contained 50 μM of the ^{15}N-labeled protein in potassium phosphate buffer (50 mM, pH 8) with 10% D_2O.

Cell Uptake Studies. The uptake of peptide-functionalized ultrasmall gold nanoparticles was carried out with human cervix carcinoma cells (HeLa). HeLa cells were cultured in Dulbecco's modified Eagle's medium (DMEM), supplemented with 10% fetal bovine serum (FBS), 100 U mL^{-1} penicillin, and 100 U mL^{-1} streptomycin at 37 °C in 5% CO_2 atmosphere. The cells were trypsinized and seeded in a glass-bottom dish (ibidi μ-Slide, Planegg, Germany) with 10^4 cells per well in 200 μL of cell culture medium 24 h prior to the uptake studies. A 20 μL portion of 125 μg mL^{-1} CGGpTPAAK-5,6-FAM-NH_2-functionalized gold nanoparticles in 180 μL cell medium were added to the cells. The final gold nanoparticle concentration was 12.5 μg mL^{-1} per well. After incubation for 24 h, HeLa cells were washed three times with 200 μL of phosphate-buffered saline (PBS) and fixed with 100 μL of 4% aqueous paraformaldehyde (PFA) for 20 min at room temperature. The PFA was removed, and the cells were washed again three times with 200 μL PBS. For a better permeabilization for the dyes, the cells were treated with 150 μL of 0.1% Triton X-100 for 5 min and then washed twice with 200 μL PBS. Cell actin was stained by incubating the cells with 200 μL of 25 μg mL^{-1} Alexa-Fluor 660-phalloidin (Invitrogen, Karlsruhe, Germany) solution in PBS with 1% bovine serum albumin for 20 min. After washing the cells with PBS, the cells were incubated for 15 min with 150 μL of a 1 μg mL^{-1} Hoechst33342 (Life Technologies, Carlsbad, CA, U.S.A) solution in PBS for nucleus staining. Afterward, the cells were washed three times with PBS and then analyzed with a Leica TCS SP8 confocal laser scanning microscope with a 63X NA1.2 water objective.

Analytical Methods. The gold concentration in the nanoparticle dispersion was determined by atomic absorption spectroscopy (AAS) with a Thermo Electron M-Series spectrometer (graphite tube furnace according to DIN EN ISO/IEC 17025:2005) after dissolving the nanoparticles in *aqua regia*.

Analytical disc centrifugation (differential centrifugal sedimentation; DCS) was performed with a CPS Instruments DC 24000 disc centrifuge (24 000 rpm). Two sucrose solutions (8 and 24 wt %) formed a density gradient that was capped with 0.5 mL dodecane as a stabilizing agent. The calibration standard was a poly(vinyl chloride) (PVC) latex in water with a particle size of 483 nm provided by CPS Instruments. A calibration was carried out prior to each run. A sample volume of 100 μL of dispersed nanoparticles was used. The recording time was about 6 h at the given centrifugation speed due to the small particle size. The density of elemental gold (19 300 kg m^{-3}) was used for the computations.

https://dx.doi.org/10.1021/acsabm.0c01424
ACS Appl. Bio Mater. 2021, 4, 945−965

UV−vis spectroscopy was performed with a Varian Cary 300 instrument from 200 to 800 nm after background solvent correction (50 mM potassium phosphate buffer, pH 8). Suprasil quartz glass cuvettes with a sample volume of 500 μL were used. Fluorescence spectroscopy was performed with an Agilent Technologies Cary Eclipse Spectrophotometer in the range of 500−700 nm. A 96-well opaque flat bottom microplate with a sample volume of 300 μL was used.

High-resolution transmission electron microscopy was performed with an aberration-corrected FEI Titan transmission electron microscope equipped with a Cs-probe corrector (CEOS Company) operating at 300 kV.[52]

The calculation of nanoparticle concentrations was carried out as follows (given here for a nanoparticle diameter of 2 nm and a gold concentration of 2.01 g L^{-1}):

$$V_{NP} = \frac{4}{3}\pi\left(\frac{d}{2}\right)^3 = \frac{4}{3} \times 3.14\left(\frac{2 \times 10^{-9}\ \text{m}}{2}\right)^3 = 4.19 \times 10^{-27}\ \text{m}^3$$

$$m_{NP} = V_{NP}\rho_{Au} = 4.19 \times 10^{-27}\ \text{m}^3 \times 19\,302\,000\ \text{g m}^{-3} = 8.09 \times 10^{-20}\ \text{g}$$

$$c_{NP} = \frac{c_{Au}}{m_{NP}} = \frac{2.01\ \text{g L}^{-1}}{8.09 \times 10^{-20}\ \text{g}} = 2.49 \times 10^{19}\ \text{L}^{-1}$$

$$N_{NP} = c_{NP}V_{sample}$$

NMR spectroscopy was performed on a Bruker Avance III 700 MHz spectrometer with a 5 mm TCI ^{1}H/^{13}C/^{15}N/D cryoprobe with a z-gradient in a 3 mm sample tube at 25 °C. All gold nanoparticle dispersions and protein solutions were prepared in 200 μL potassium phosphate buffer (50 mM, pH 8) and D_2O (90:10 volume ratio). The ^{1}H-DOSY pulse sequence from the Bruker library was modified by adding a presaturation pulse to suppress the remaining water signal. For the DOSY experiments, a diffusion time Δ of 100 ms was chosen, and the pulsed gradient duration δ was 3 ms for the free peptide and 4 ms for the peptide-conjugated gold nanoparticles. For each pseudo-2D DOSY data set, the gradient strength was incrementally increased from 5 to 95% (maximum gradient strength 50.4 G cm^{-1} for a smoothed square gradient pulse) in 32 steps with a linear ramp. The spectra were Fourier-transformed, phased, and integrated with the program Topspin versions 3.5 and 4.0.4 (Bruker). Plotting and fitting of the linearized diffusion data according to the Stejskal−Tanner equation[53,54]

$$\ln\left(\frac{I}{I_0}\right) = -\gamma^2\delta^2(\Delta - \delta/3)DG^2 \quad (1)$$

were performed with IGOR Pro (WaveMetrics, Inc.) with I as the signal intensity, I_0 as the signal intensity without gradient, γ as the gyromagnetic ratio of ^{1}H, δ as the diffusion gradient pulse length, Δ as the diffusion delay, G as the gradient strength, and D as the translational diffusion coefficient.

The Stejskal−Tanner plots of three well-discernible proton signals of the peptide and of the peptide-functionalized gold nanoparticles were first analyzed separately. Upon yielding the same diffusion coefficient within the error margin, the relative intensities I/I_0 of all signals were averaged for dissolved peptide and nanoparticle-conjugated peptide, respectively. Error bars of the averaged data points represent the standard deviation of these proton signals. The accuracy of the diffusion coefficient was determined by averaging the errors obtained from the 2D-^{1}H-DOSY spectrum.

The hydrodynamic diameter was calculated by the Stokes−Einstein equation

$$d_H = \frac{kT}{3\pi\eta D} \quad (2)$$

with d_H as the hydrodynamic diameter, k as the Boltzmann constant, T as the temperature in K, $\eta\delta$ as the dynamic viscosity of H_2O at 25 °C, and D as the translational diffusion coefficient.

Quantitative ^{1}H NMR spectroscopy and ^{15}N NMR spectroscopy were performed with a Bruker-AVANCE III 600 MHz spectrometer equipped with a Prodigy cryoprobe head in a 5 mm Shigemi tube with 400 μL sample volume in D_2O at 25 °C. The concentration was determined by the ERETIC (electronic reference to access *in vivo* concentrations) method, and maleic acid was used as an external standard.[55]

The interaction between peptide and functionalized nanoparticles and the WW domain of the hPin1 protein was investigated by ^{1}H−^{15}N-HSQC NMR spectroscopy titrations. To 200 μL of ^{15}N-labeled hPin1-WW (in potassium phosphate buffer, pH 8) or ^{15}N-labeled gold nanoparticles, either a 200 μL unlabeled peptide-functionalized gold nanoparticle dispersion or unlabeled hPin1-WW was titrated stepwise, respectively. The resulting difference in the chemical shift was calculated by eq 3:[56]

$$\Delta\delta_{max} = \sqrt{(\Delta H_N)^2 + (1.54 \cdot \Delta N)^2} \quad (3)$$

The dissociation constant K_D is defined as the equilibrium constant for the reaction

$$\text{protein−peptide (aq)} \leftarrow\rightarrow \text{protein (aq)} + \text{peptide (aq)} \quad (4)$$

i.e.

$$K_D = \frac{[\text{protein−peptide (aq)}]}{[\text{protein (aq)}][\text{peptide (aq)}]} \quad (5)$$

with protein−peptide as the complex of protein and peptide.

K_D was determined by fitting the chemical shift difference to the following quadratic equation, assuming a one-site specific binding model:

$$\Delta\delta_{obs} = \Delta\delta_{max} \frac{([P_0] + [[L_0] + [K_D]]) - \sqrt{([P_0] + [L_0] + K_D)^2 - 4[P_0][L_0]}}{2[P_0]} \quad (6)$$

where $\Delta\delta_{obs}$ is the difference in the observed shift from the unbound state, $\Delta\delta_{max}$ is the maximum chemical shift difference at the saturation point, P_0 is the concentration of the ^{15}N-labeled signal-giving analyte (protein or ligand), L_0 is the concentration of the unlabeled titrant (ligand or protein being titrated in), and K_D is the dissociation constant.[57]

Isothermal titration calorimetry (ITC) was performed with a MicroCAL iTC200 (Malvern Panalytical) instrument in potassium phosphate buffer (50 mM, pH 8) at 25 °C. In the sample cell, 300 μL of hPin1-WW (10−100 μM, corresponding to 0.003−0.03 μmol protein) was titrated with a peptide-functionalized gold nanoparticle dispersion. The first injection volume was 0.4 μL with a mixing time of 2 s and a time interval of 110 s. Then, 35 injections of 1 μL aliquots of the nanoparticle dispersion followed with a mixing time of 2 s and a time interval of 110 s, respectively. The measurements were carried out with an initial delay of 60 s, a reference power of 5 μcal s^{-1}, a stirring power of 750 rpm, and a filter period of 3 s. The dissociation constant ($K_D = 1/K_A$), the molar binding stoichiometry (N), and the molar binding enthalpy (ΔH^0) were calculated by integrating the peaks obtained from Enthalpy changes and presenting them in a Wiseman plot.[58] A one-set-of-sites specific-binding model was assumed. Points 2−35 were fit by the Hill equation

$$H = H_0 + (H_{max} - H_0)\left(1 + \left(\frac{N}{n}\right)^{K_D}\right)^{-1} \quad (7)$$

with H as the molar heat per injection volume, H_0 as the molar heat at the beginning of the measurement, H_{max} as the maximum measured molar heat, n as the molar ratio of peptides to proteins, and N as the molar binding stoichiometry. Here, the point of inflection gives the molar binding stoichiometry, and the slope at the point of inflection is K_D. All data analyses were done with IGOR Pro.

https://dx.doi.org/10.1021/acsabm.0c01424
ACS Appl. Bio Mater. 2021, 4, 945−965

Fluorescence polarization (FP) was performed with a JASCO FP-8300 fluorescence spectrometer in potassium phosphate buffer (50 mM, pH 8) at 20 °C in Suprasil quartz glass cuvettes with a sample volume of 60 μL. hPin1-WW was added stepwise to the peptide and the peptide-functionalized gold nanoparticles, respectively. The resulting anisotropy at the emission wavelength of 520 nm was measured by exciting the sample with linearly polarized light at 500 nm. Fitting for the K_D determination was done with IGOR Pro with the following quadratic binding equation for a one-site specific binding model

$$r = r_0 + r_{max} \frac{([FL] + [[P] + [K_D]]) - \sqrt{([FL] + [P] + K_D)^2 - 4[FL]}}{2[FL]} \quad (8)$$

with r as the anisotropy, r_0 as the anisotropy without protein, r_{max} as the maximum anisotropy, FL as the concentration of the analyte (fluorescently labeled ligand), P as the concentration of the added titrant (protein), and K_D as the dissociation constant.

SAXS measurements were performed on a laboratory Xenocs-XEUSS2.0 instrument at the Institute of Physics, University of São Paulo. This equipment was equipped with a Genix3D Cu Kα source (λ = 0.15418 nm), Fox3D focusing mirrors and two sets of scatterless slits. 2D scattering images were collected on a Pilatus 300 k detector. The integration of the 2D SAXS patterns was done with the FIT2D software.[59] Pure water was used for blank scattering subtraction. Error estimation and normalization to an absolute scale were performed with a self-written software. The obtained 1D curves give the scattering intensity as a function of the reciprocal space momentum transfer modulus $q = 4\pi(\sin\theta)/\lambda$, where 2θ is the scattering angle. The sample-to-detector distance used on the experiments was 1.200 m which gave a q range of $0.1 < q < 3.2$ nm^{-1}. Data treatment and normalization to absolute scale were performed by standard procedures.[60,61] In some cases, a few points in the beginning were clipped due to problems with the background subtraction.

The dissolved protein hPin1-WW was analyzed by SAXS as follows: The hPin1-WW concentration was 2.65 mM, corresponding to 12.06 g L^{-1} for a molecular weight of 4,551 g mol^{-1}. From the IFT modeling we obtained a forward scattering $I(0) = 0.0337(1)$ cm^{-1}. For proteins in solution one can use the molar concentration of the proteins, the electron density contrast for the proteins in solution, and the protein volume. However, since the protein volume is not easily accessible, it is easier to use the protein molecular weight which is related to the protein volume as

$$V = \upsilon M_W \quad (9)$$

with υ as the partial specific volume of the protein (volume per mass). For proteins, a typical value is υ = 0.72 cm^3 g^{-1}. Then, we can write[60]

$$I(q)_{absolute} = c\Delta\rho_M{}^2 \left(\frac{M_W}{N_A}\right) P(q)S(q)\ [cm^{-1}] \quad (10)$$

and

$$I(0)_{absolute} = c\Delta\rho_M{}^2 \left(\frac{M_W}{N_A}\right) [cm^{-1}] \quad (11)$$

with c as the concentration (mg mL^{-1}), M_W as the molecular weight (kDa), and $\Delta\rho_M$ as the protein excess scattering length contrast $\Delta\rho_M = 2 \times 10^{10}$ cm g^{-1}.[60] From eq 11 it is possible to calculate the molecular weight of hPin1-WW as 4200 ± 350 g mol^{-1} which is very close to the expected value of 4551 g mol^{-1}.

For the analysis of the SAXS data for the protein, the indirect Fourier transformation (IFT) method was used, in a slightly different implementation.[62] The obtained pair distance distribution function $p(r)$ indicates the overall shape of the protein. Also, one obtains the radius of gyration of the protein R_G and the forward intensity $I(0)$. The latter information is useful for the estimation of the molecular weight of the protein.

Since the PDB model for the protein was known (PDB ID: 2M8I),[63] it was possible to compare the atomic resolution structure with the experimental SAXS data. For this comparison, the program Crysol[64] was used. The model could not describe the initial part of the SAXS data, indicating differences on the protein shape or presence of a small fraction of oligomers. As shown below, the introduction of a fraction of dimers[65] resulted in a perfect fit of the SAXS data.

For a protein/nanoparticle complex, the much higher electron density contrast of the crystalline gold nanoparticle (~4.3 el Å^{-3} compared to the protein in solution (~0.1 el Å^{-3}) makes the contribution of the NP dominant for the scattering of X-rays, even for the ultrasmall (~2 nm) gold NP. Therefore, SAXS is a very good probe for the gold nanoparticles in the system, even in the case of a protein/nanoparticle complex. In addition, it is possible to monitor the formation of nanoparticle aggregates which might form via protein cross-linking.

For the modeling of protein/nanoparticle complexes, the IFT method was used, but now assuming a polydisperse system of spheres. The calculations were performed with the program GNOM.[66] As a result one obtains the volume-weighted radius distribution for the particles in the system.

RESULTS AND DISCUSSION

The ultrasmall gold nanoparticles were surface-functionalized with selected peptides to target the WW domain of the protein hPin1. We have attached the following synthetic model peptides which contain the pTP recognition motif for the WW domain: CGGpTPA as binder to the hPin1-WW domain, CGGpTP(A*-^{15}N) labeled with ^{15}N in the alanine residue only, CGGpTPAAK-(5,6)-FAM-NH$_2$ as fluorescently labeled derivative, CGSGGGpTPA as binder to hPin1 with three additional amino acids as spacers, and CGSGGGTDA as control peptide (no binding to hPin1-WW). The attachment of the peptides occurs by the stable terminal cysteine-sulfur bond to the gold nanoparticle surface, whereas the phosphothreonine/proline pTP motif is the binding site for hPin1-WW.

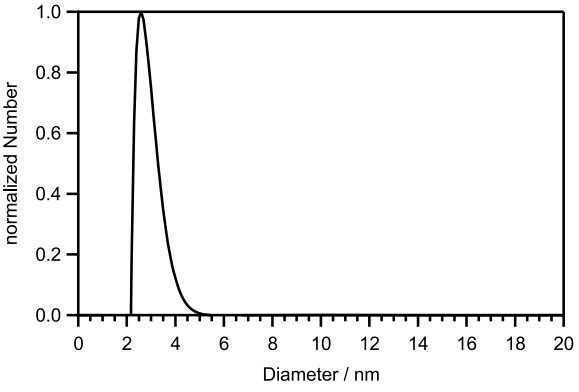

Figure 1. Representative particle size distribution of Au-CGGpTPA nanoparticles measured by differential centrifugal sedimentation (DCS). For the other peptide-conjugated nanoparticles, similar results were obtained (see Figures S1−S3).

Differential centrifugal sedimentation (DCS) gave a hydrodynamic diameter of about 3.0 nm for peptide-conjugated gold nanoparticles (Figure 1). It must be stressed that the ligand shell on the particles generally influences the effective density, especially for ultrasmall nanoparticles: The ligand shell has a much lower density than the gold core and leads to a lower

https://dx.doi.org/10.1021/acsabm.0c01424
ACS Appl. Bio Mater. 2021, 4, 945−965

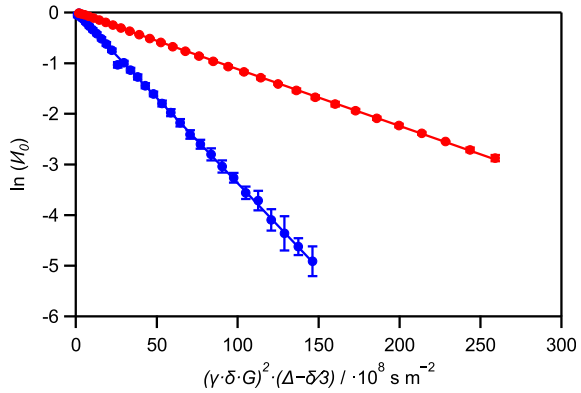

Figure 2. ^{1}H-DOSY hydrodynamic radii of dispersed nanoparticles and dissolved peptides. Representative Stejskal−Tanner plot of the hexapeptide CGGpTPA alone(**blue**) and of Au-CGGpTPA nanoparticles (**red**). For the other peptide-conjugated nanoparticles, similar results were obtained (see Figures S4−S7).

sedimentation rate and consequently a systematic underestimation of the hydrodynamic particle diameter.[67] Thus, the DCS data only demonstrate that the particles are not agglomerated, but their quantitative value is limited. Dynamic light scattering (DLS) was not possible due to the very small particle size. The hydrodynamic diameter of dissolved peptides and peptide-coated nanoparticles was also measured by ^{1}H-DOSY NMR (Figure 2).

High-resolution transmission electron microscopy gave the diameter of the metallic core of the peptide-conjugated gold nanoparticles (Figure 3). The particles were crystalline with a core diameter of about 2 nm.

The good particle dispersion was also assessed by small-angle X-ray scattering (SAXS) (Figures 4 and 5). The peptide-conjugated gold nanoparticles were stable without the presence of aggregates. For the Au-CGGpTPA sample there was a main contribution with a core diameter of ∼2 nm which is in agreement with the size of the nanoparticles. For Au-CGSGGGpTPA, the main contribution to the size distribution was at ∼1.4 nm which is also in agreement with the results obtained from the other methods. In both cases there were small fractions at higher radius but the number fraction of such larger particles was very small.

For comparison, we also analyzed the dissolved protein hPin1-WW by SAXS (Figure 6). There were clear indications for the presence of protein dimers. However, these are likely due to the high concentrations used for SAXS as we did not observe significant NMR line broadening, which would indicate an increase in molecular size, up to a concentration of 1 mM. The atomic resolution structure of this protein is known and can be compared with the solution scattering data. The comparison of the atomic resolution structure and the SAXS data is shown in Figure 7. The model cannot describe the initial part of the SAXS data. By assuming a coexisting fraction of monomers and dimers,[65] we obtained a perfect fit of the SAXS data with number fractions of 90% monomers and 10% dimers, with a distance between the protein centers of ∼2.73 nm. A tentative arrangement of the dimers is also shown in Figure 7. Note that the protein does not contain cysteine, therefore the formation of disulfide bridges can be excluded.

Table 1 comprises all size characterization data of dissolved hPin1-WW, of the dissolved peptides, and of the peptide-conjugated gold nanoparticles.

The hydrodynamic diameter of the peptide-conjugated nanoparticles from ^{1}H-DOSY is about 5 nm. Considering the diameter of the metallic core from HRTEM of 2 nm, we obtain a thickness of the hydrated peptide layer about 1.5 nm around each nanoparticle. This is in a good agreement with the hydrodynamic diameter of the dissolved peptides by ^{1}H-DOSY that is in the range of 1.3−2.3 nm. There are only small differences between the differently functionalized nanoparticles. Note that the hydrodynamic diameter increases with increasing peptide length but that the diameter of the gold core remains constant with about 2 nm (HRTEM, SAXS). This confirms that the metal core is not affected by the surface-conjugation of the peptides.

Unlike with bigger nanoparticles, NMR spectroscopy is possible for ultrasmall nanoparticles, although signal broadening and line shifts may complicate the interpretation.[43−45,68,69] ^{1}H NMR spectra clearly showed the binding of the peptide to the gold nanoparticles. In all cases, cysteine protons were considerably affected by the presence of the metallic gold whereas the other amino acids were less influenced due to the higher distance from the gold surface (Figure 8).[68] No disulfide was observed in the nanoparticle dispersion. Disulfide signals of the cystine (cysteine disulfide) β-protons are typically located between 3.0 and 3.2 ppm.

^{15}N NMR spectra of ^{15}N-labeled CGGpTPA on the surface of gold nanoparticles showed no significant change in the chemical shift or a broadening of the ^{15}N-signal of the terminal alanine, in contrast to the ^{1}H-signals of the cysteine protons (Figure 9). Therefore, we exclude an interaction on the

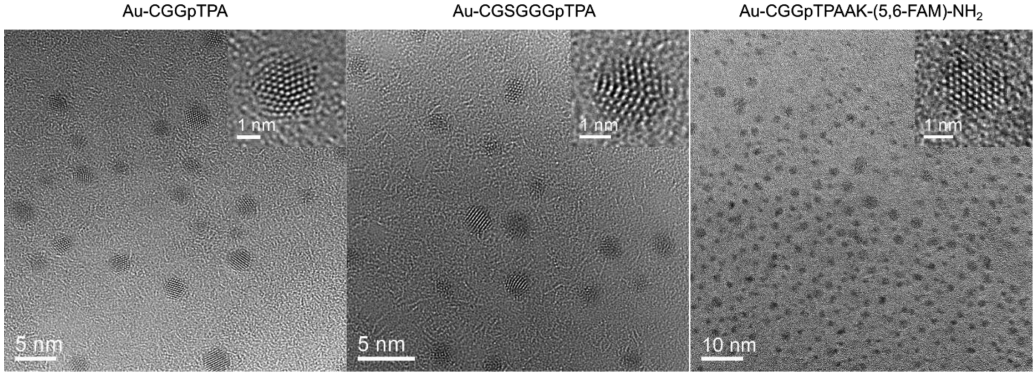

Figure 3. High-resolution transmission electron microscopy (HRTEM) of peptide-conjugated ultrasmall gold nanoparticles: Au-CGGpTPA, Au-CGSGGGpTPA, and Au-CGGpTPAAK-(5,6-FAM)-NH_2.

https://dx.doi.org/10.1021/acsabm.0c01424
ACS Appl. Bio Mater. 2021, 4, 945−965

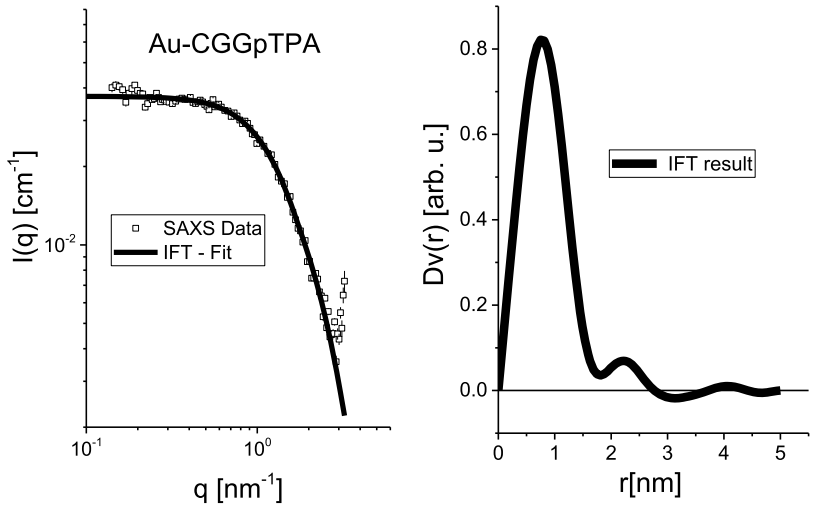

Figure 4. SAXS results of Au-CGGpTPA nanoparticles. (**left**) SAXS data (symbols) and IFT-fit using a polydisperse system of hard spheres (solid lines). (**right**) Volume-weighted radius distribution.

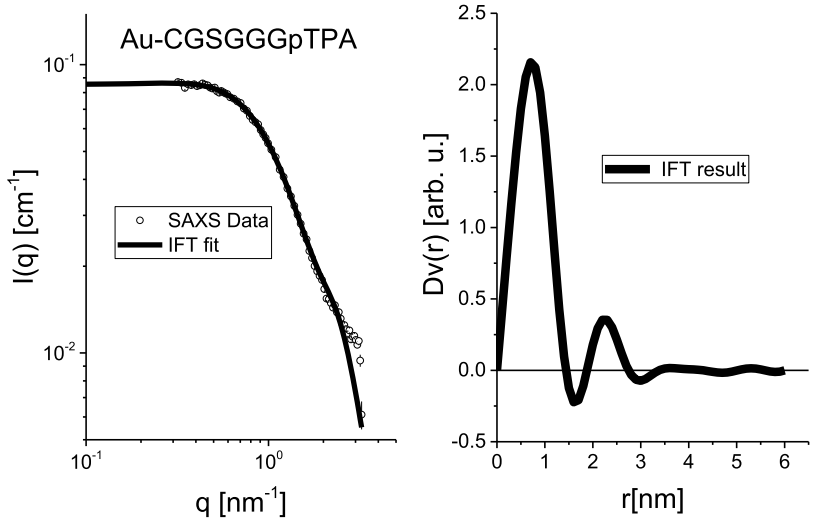

Figure 5. SAXS results of Au-CGSGGGpTPA nanoparticles. (**left**) SAXS data (symbols) and IFT-fit using a polydisperse system of hard spheres (solid lines). (**right**) Volume-weighted radius distribution.

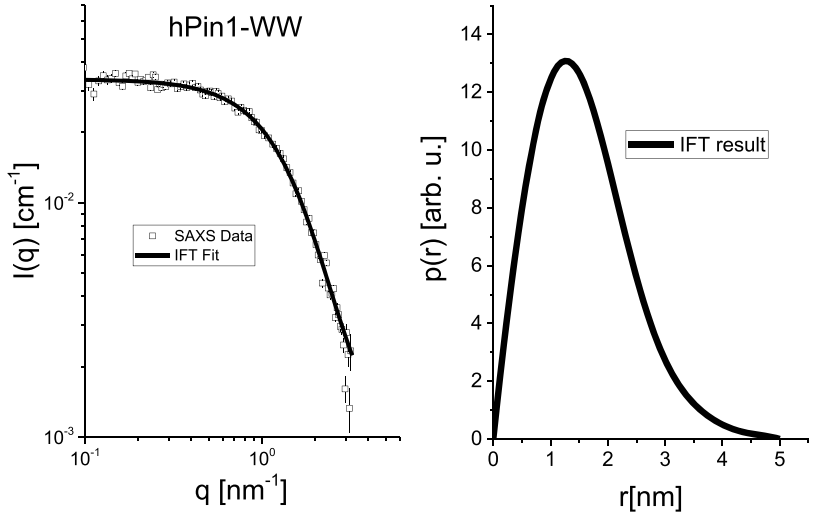

Figure 6. SAXS investigation of the dissolved protein hPin1-WW. (**left**) SAXS data (symbols) and IFT-fit assuming a monodisperse system (solid lines). (**right**) Pair distance distribution function $p(r)$ for hPin1-WW.

https://dx.doi.org/10.1021/acsabm.0c01424
ACS Appl. Bio Mater. 2021, 4, 945−965

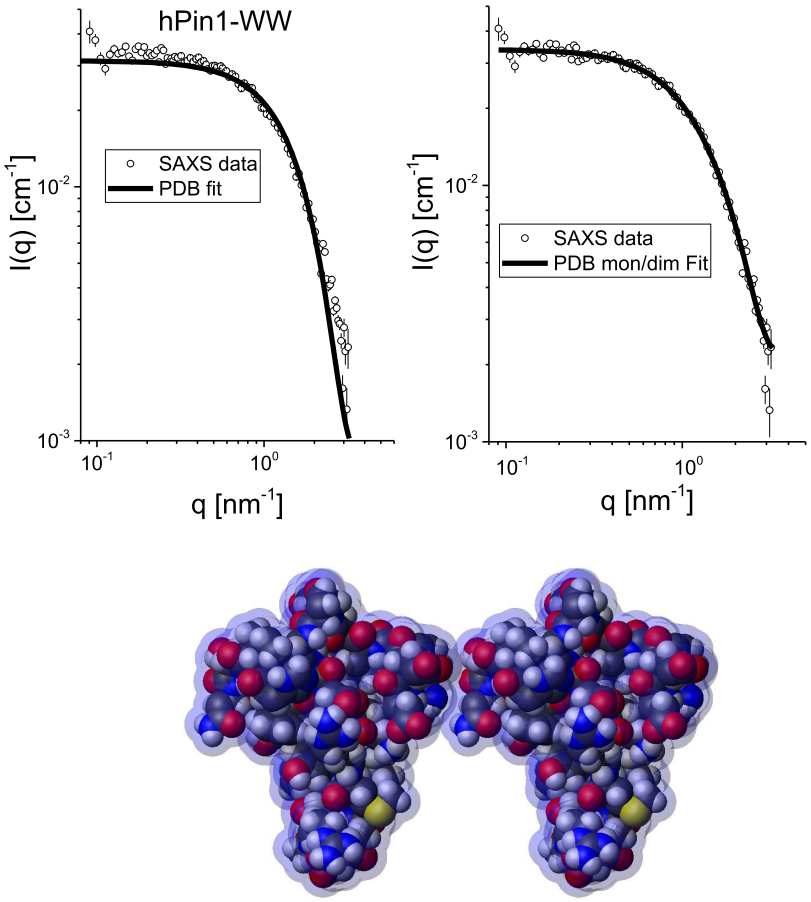

Figure 7. Fit of SAXS data of dissolved hPin1-WW, using the atomic resolution structure from the protein database (PDB ID: 2M8I). (**top left**) Comparison of the SAXS data with the atomic resolution structure. Clearly, the theoretical fit does not match the initial part of the SAXS data. (**top right**) Fit assuming the presence of 90% monomers and 10% dimers. (**bottom**) Tentative dimer arrangement of hPin1-WW monomers, including the hydration shell around the proteins in light blue. Note that this image just illustrates the size of a dimer without taking into account possible interactions between the two protein molecules.

Table 1. Properties of the Dissolved Protein hPin1-WW, of the Dissolved Peptides, and of Peptide-Conjugated Ultrasmall Gold Nanoparticles from ^{1}H-DOSY, DCS, HRTEM, and SAXS[a]

	D (^{1}H-DOSY)/10^{-10} m^2 s^{-1}	d_h (^{1}H-DOSY)/nm	d_h (DCS)/nm	d_{core} (HRTEM)/nm	$2r_{saxs}$ (SAXS)/nm[b]
hPin1-WW protein	1.7 ± 0.2	2.9 ± 0.3			3.22 ± 0.03
CGGpTPA peptide	3.4 ± 0.4	1.4 ± 0.2			
Au-CGGpTPA nanoparticle	1.1 ± 0.1	4.4 ± 0.4	3.4 ± 0.4	2.0 ± 0.4	1.6 ± 0.5
CGSGGGpTPA peptide	3.0 ± 0.3	1.6 ± 0.2			
CGGpTP(A-^{15}N) peptide	3.5 ± 0.4	1.4 ± 0.1			
Au-CGGpTP(A-^{15}N) nanoparticle	1.1 ± 0.1	4.3 ± 0.4	2.7 ± 0.7		
Au-CGSGGGpTPA nanoparticle	0.9 ± 0.1	5.4 ± 0.5	3.0 ± 0.9	2.0 ± 0.4	2.6 ± 0.9
CGSGGGTDA peptide	3.2 ± 0.3	1.5 ± 0.2			
Au-CGSGGGTDA nanoparticle	0.9 ± 0.1	5.3 ± 0.5	3.1 ± 0.7		
CGGpTPAAK-(5,6)-FAM-NH_2 peptide	2.4 ± 0.2	2.0 ± 0.2			
Au-CGGpTPAAK-(5,6)-FAM-NH_2 nanoparticle	1.0 ± 0.1	5.0 ± 0.5	2.0 ± 0.7	2.0 ± 0.6	

[a]An error of 10% for the diffusion coefficient and the hydrodynamic diameter measured by ^{1}H-DOSY was assumed. Note that DCS systematically underestimates the particle diameter. For the HRTEM data, between 80 and 100 particles were analyzed, and the average diameter and the standard deviation were computed. [b]Radius of the equivalent sphere with the same radius of gyration, $r_{saxs} = \sqrt{\frac{5}{3}} R_G$

millisecond time scale between the alanine-nitrogen and the gold nanoparticle surface, like a back-folding of the peptide chain.

The ^{1}H−^{1}H-TOCSY spectrum of the unbound peptide showed a clear correlation pattern of the α- and β-protons of cysteine whereas the cross-peaks of correlated cysteine-protons of the nanoparticle-conjugated peptide were no longer visible due to strong line broadening in the presence of the gold surface (Figure 10). In addition, it is possible that the cysteine signals are now overlapping with the H_α signals of the other residues. Such strong line broadening, along with a large shifting, of the signals compared to free cysteine was observed

https://dx.doi.org/10.1021/acsabm.0c01424
ACS Appl. Bio Mater. 2021, 4, 945−965

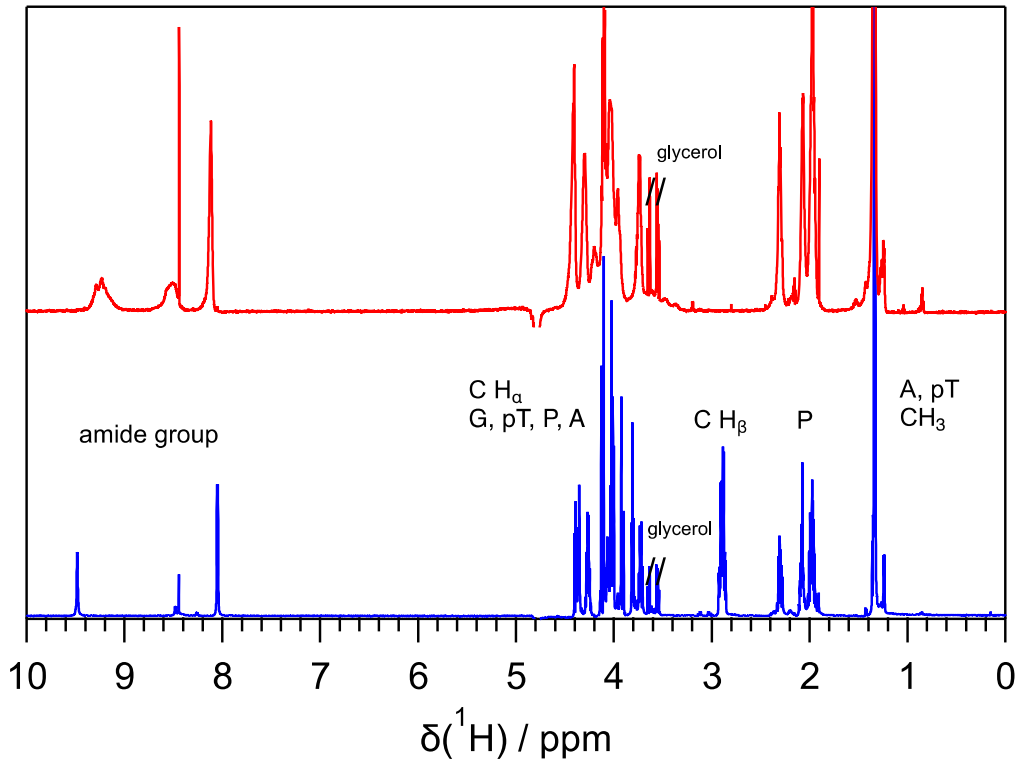

Figure 8. Representative ^{1}H NMR spectra of Au-CGGpTPA nanoparticles (**top**) and of the dissolved peptide CGGpTPA (**bottom**). The spectra of the other peptides (free and bound to gold nanoparticles) are shown in the Supporting Information (Figures S8−S10).

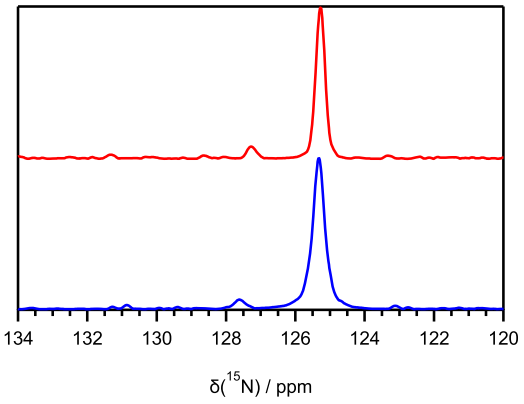

Figure 9. ^{15}N NMR spectra (taken from ^{1}H−^{15}N-HSQC spectra) of Au-CGGpTP(A-^{15}N) nanoparticles (**top**) and of the dissolved CGGpTP(A-^{15}N) peptide (**bottom**). The ^{15}N signal of the terminal alanine is not influenced by the conjugation to the gold nanoparticles, indicating that no back-folding to the gold surface occurs.

earlier on cysteine-conjugated gold nanoparticles.[68] The fact that the proton couplings of the other amino acids were mostly unchanged confirms that the peptide chain was still intact after binding to the gold nanoparticles. These residues experience less severe line broadening because they are more distant from the gold core and also show a higher mobility, and thus slower T2-relaxation, compared to the gold-bound cysteine. Some correlation peaks were not visible due to the signal-to-noise ratio, overlap with the water signal and peak broadening. The glycerol in the nanoparticle sample was an impurity from the spin filter.

To assess the binding of the peptide-conjugated nanoparticle to the protein, it is important to know how many peptide molecules are bound to each nanoparticle. The surface loading of the gold nanoparticles was determined by UV−vis spectroscopy after conjugation of a fluorescent derivative of the peptide (Figure 11). With a gold nanoparticle diameter of 2 nm, this leads to about 129 CGGpTPAAK-(5,6-FAM)-NH_2 molecules on each nanoparticle (molecular footprint 0.10 nm^2).

The amount of bound CGSGGGpTPA peptide was confirmed by quantitative ^{1}H NMR spectroscopy with maleic acid as external standard. The peptide concentration was computed from the methyl groups of alanine and threonine at 1.37 ppm to 0.42 mM. This corresponds to 168 nmol peptide in a gold nanoparticle dispersion with a gold concentration of 0.12 g L^{-1} given by AAS. With an average nanoparticle diameter of 2 nm, a gold nanoparticle concentration of 2.38 μM with 176 peptide molecules per nanoparticle were derived (footprint 0.071 nm^2). This is in reasonable agreement with the above result from UV−vis spectroscopy. If we take the average of the results by UV spectroscopy and NMR spectroscopy, about 150 peptide molecules are bound to each nanoparticle, giving a footprint of about 0.084 nm^2 per peptide molecule. Clearly, these values are associated with a considerable degree of error because the particles are not all of the same size, because they are not strictly spherical, because the density of small gold particles may be lower than that of bulk gold and because the applied methods (UV and NMR) also carry an error on their own. The individual methodological errors are not known, but it is reasonable to assume that the number of 150 peptides per nanoparticles is associated with an error of 30%, giving an average of 150 ± 45 peptide molecules per nanoparticle. Of course, this variance has to be kept in mind when further calculations (like K_D values or molecular footprints) are considered.

https://dx.doi.org/10.1021/acsabm.0c01424
ACS Appl. Bio Mater. 2021, 4, 945−965

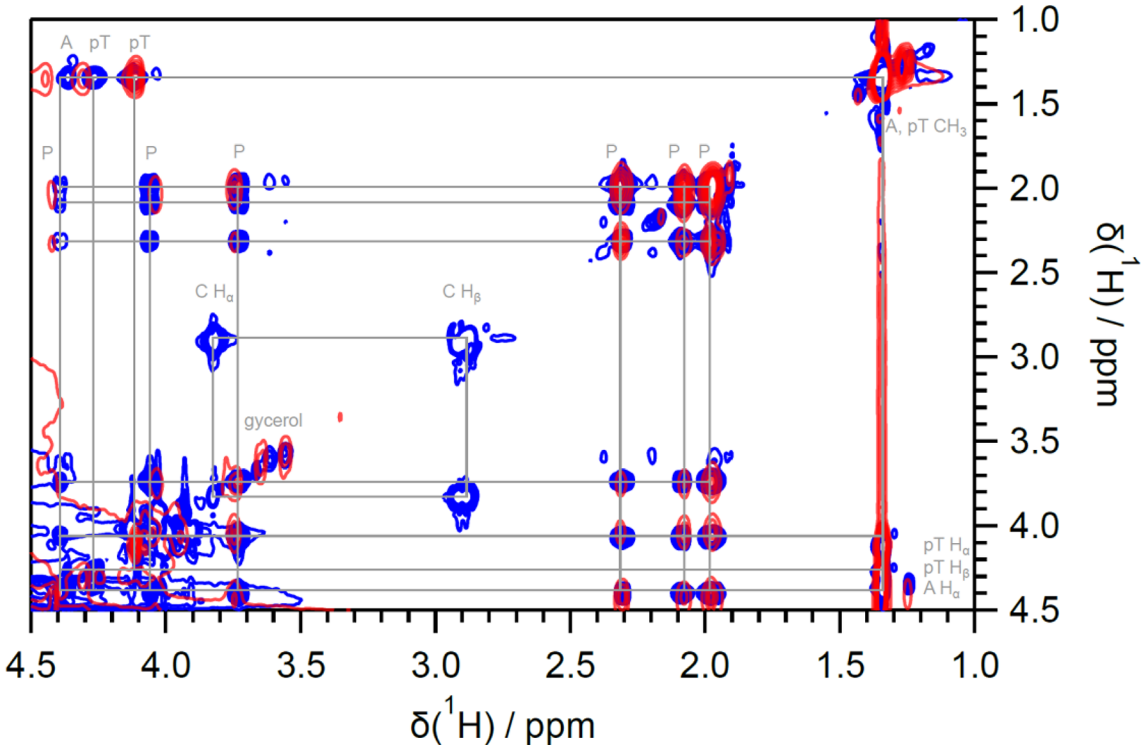

Figure 10. Overlay of $^{1}H-^{1}H$-TOCSY spectra of free CGGpTPA (**blue**) and Au-CGGpTPA nanoparticles (**red**).

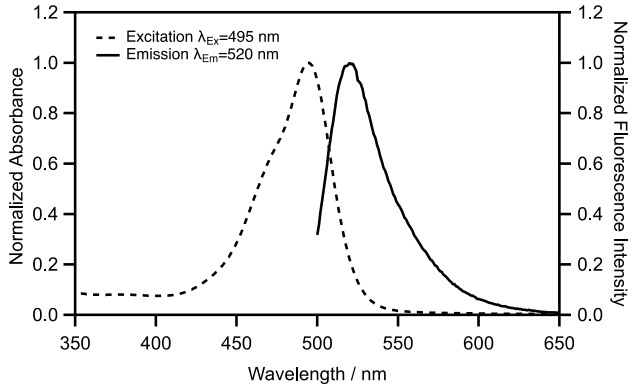

Figure 11. UV−vis spectroscopy and fluorescence spectroscopy to determine the surface loading in Au-CGGpTPAAK-(5,6-FAM)-NH_2 nanoparticles. The excitation and emission bands of the attached fluorescent peptide are shown. By recording a calibration curve beforehand and by measuring the gold content of the dispersion, the ratio of FAM-labeled peptides (c = 838 μM) and gold nanoparticles (c = 6.5 μM; diameter 2 nm) was determined to 838/6.5 = 129. Note that fluorescence quenching by the gold core as observed earlier[10] does not affect the UV absorption spectrum.

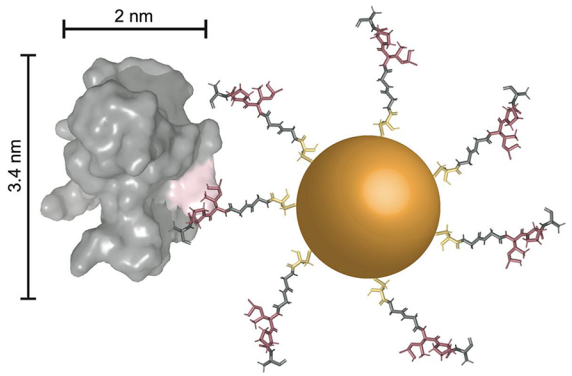

Figure 12. Schematic representation of a CGGpTPA-functionalized gold nanoparticle (2 nm) that binds to one hPin1-WW protein. The binding site on the protein is highlighted in pink.

Earlier, we had determined the footprint of a cysteine molecule on $Au_{ca.174}(cysteine)_{ca.67}$ nanoparticles (1.8 nm) with about 0.15 nm^2.[68] The packing of the peptide is almost two times higher which may be due to intermolecular noncovalent interactions that make the peptide units come closer. The data reported here are in good agreement with data found with similar systems, i.e. a molecular footprint of 0.074 nm^2 per cysteine in cysteine-bearing precision macromolecules[70] and of 0.41 nm^2 for the peptide CRaf with 36 amino acids, bound via a cysteine.[71] For all subsequent calculations and considerations, we assumed that the peptide concentration c(peptide) was 150 times the gold nanoparticle concentration c(AuNP).

The specific binding of the nanoparticle-conjugated peptides to the protein hPin1-WW is envisioned as depicted in Figure 12. We estimated the binding stoichiometry between nanoparticles and proteins as follows: An area (footprint) of 4 nm^2 to bind a hPin1-WW molecule was approximated from its steric requirement. This was done rendering the spatial structure of the domain with Pymol (The PyMOL Molecular Graphics System, Version 2.0 Schrödinger, LLC) and then estimating the area of a protein attaching via its binding site (highlighted in pink). Of course, the nanoparticle is binding to the protein not from its metallic core (about 2 nm) but from the surface after peptide conjugation. The latter can be approximated from the hydrodynamic diameter of the nanoparticle. With a protein footprint of 4 nm^2 and a hydrodynamic nanoparticle diameter of 5 nm, the maximum number of bound WW domains can be estimated. If a spherical nanoparticle is assumed, we obtain

https://dx.doi.org/10.1021/acsabm.0c01424
ACS Appl. Bio Mater. 2021, 4, 945−965

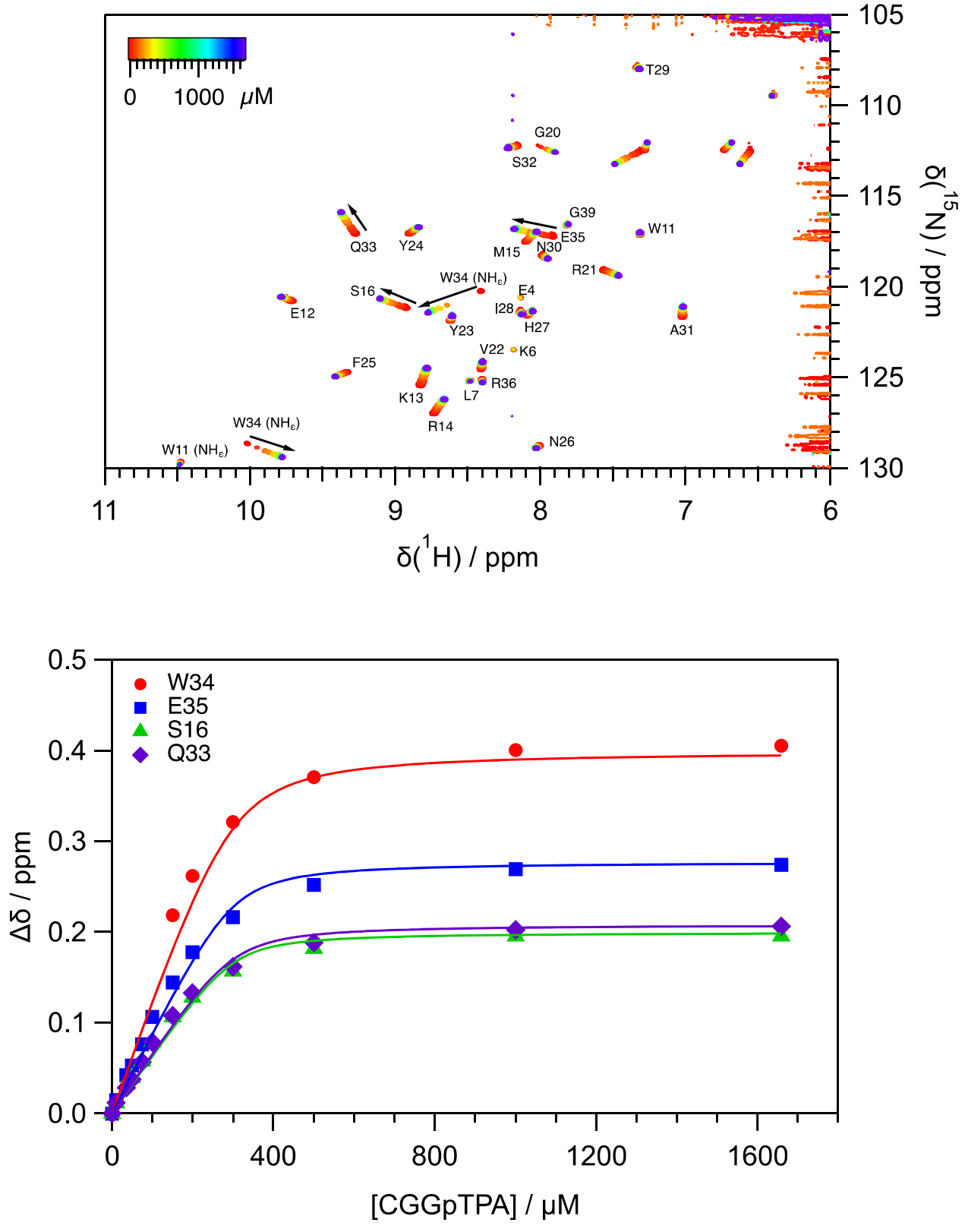

Figure 13. Overlay of $^{1}H-^{15}N$-HSQC spectra of the ^{15}N-labeled hPin1-WW (c(hPin1-WW) = 300 μM, 200 μL), titrated with CGGpTPA (c(peptide) = 4 mM, total added volume 142 μL) at pH 8 in potassium phosphate buffer. The color coding corresponds to the total peptide concentration after consideration of dilution (**top**). The total signal shifts of the amino acids S16, Q33, W34, and E35 were plotted against the peptide concentration (**bottom**) and binding curves (solid lines) were fitted.

$$N_{\text{hPin1-WW}} = \frac{4\pi r^2}{A} = \frac{4\pi \times 2.5\ \text{nm}^2}{4\ \text{nm}^2} \approx 20 \qquad (12)$$

Thus, about 20 hPin1-WW units can bind to each peptide-functionalized gold nanoparticle from a geometrical perspective. If we now take 150 peptide molecules per nanoparticle,

https://dx.doi.org/10.1021/acsabm.0c01424
ACS Appl. Bio Mater. 2021, 4, 945−965

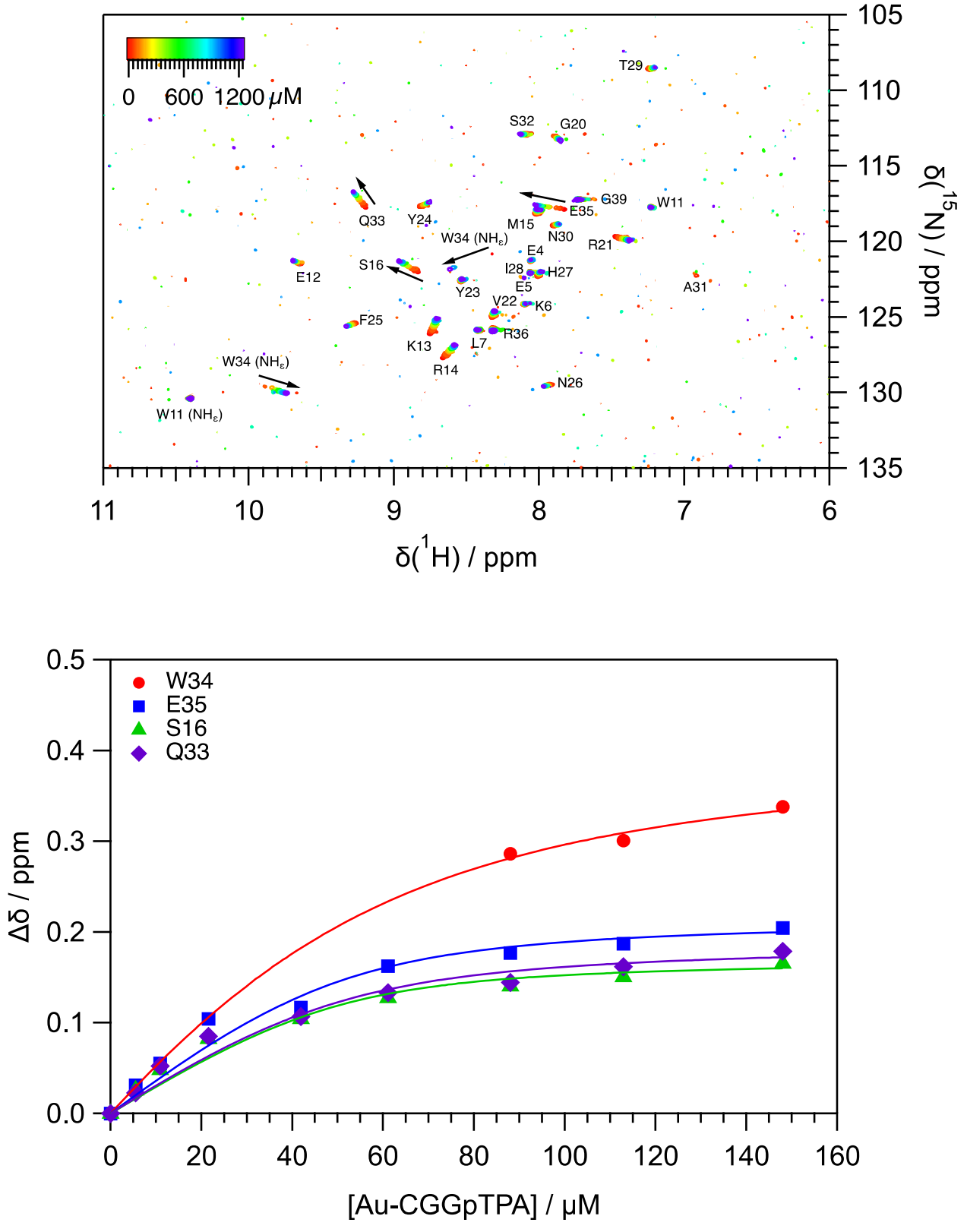

Figure 14. Overlay of $^{1}H-^{15}N$-HSQC spectra of the ^{15}N-WW domain (c(hPin1) = 50 μM, 200 μL) titrated with Au-CGGpTPA nanoparticles (c(AuNP) = 41.5 μM, c(peptide) = 6.2 mM, final added volume 50 μL) at pH 8 in potassium phosphate buffer. The peptide concentration at the end was 1.24 mM. The color coding corresponds to the total peptide concentration after consideration of dilution (**top**). The total signal shifts for the amino acids S16, Q33, W34, and E35 were plotted against the effective peptide concentration which is the actual peptide concentration divided by 8.4 (see text) (**bottom**) and binding curves (solid lines) were fitted.

about every seventh to eighth peptide molecule can bind to a protein which appears geometrically reasonable. However, it is not known whether a complex of one nanoparticle and 20 protein molecules is really stable in dispersion. This can only

https://dx.doi.org/10.1021/acsabm.0c01424
ACS Appl. Bio Mater. 2021, 4, 945−965

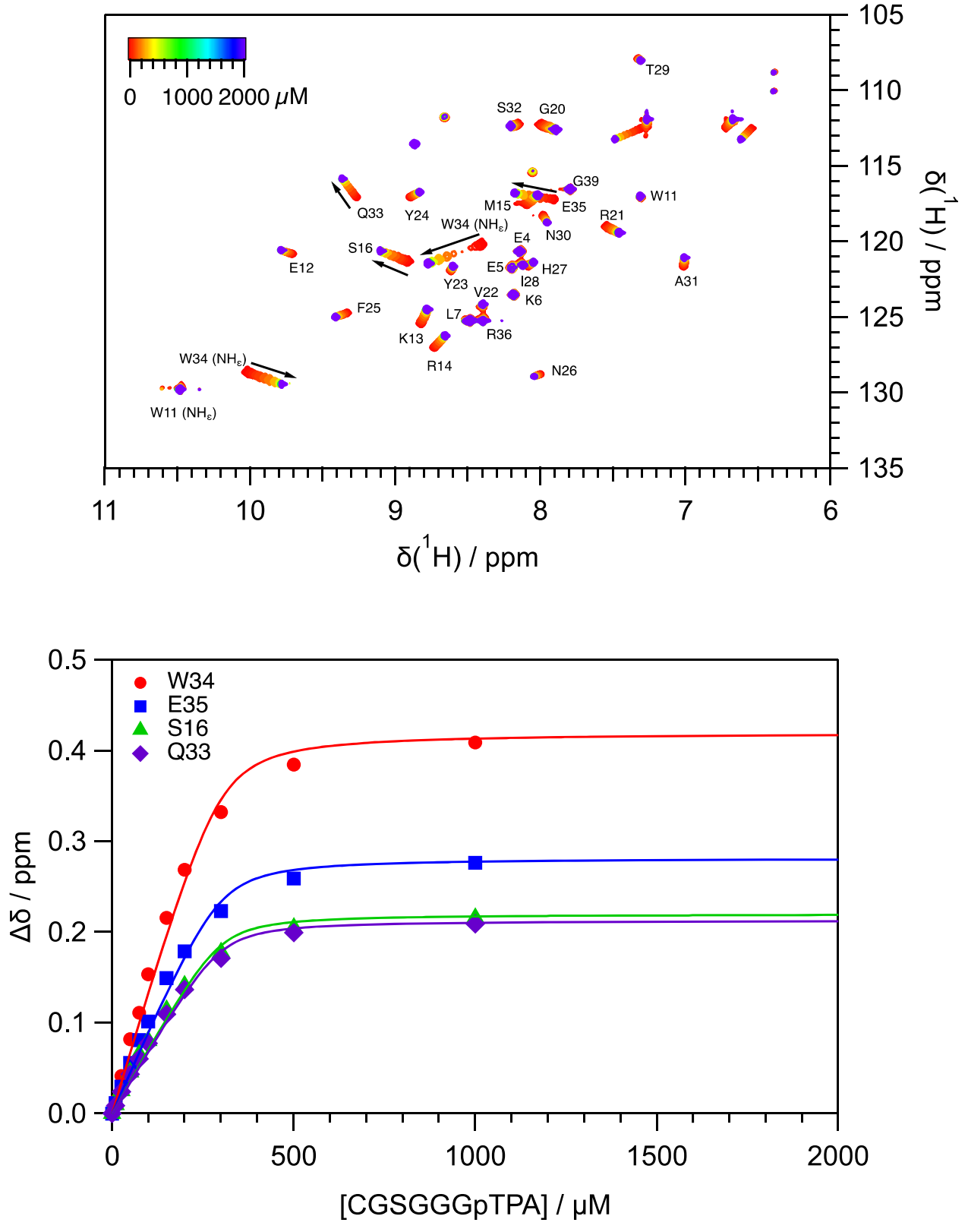

Figure 15. Overlay of $^{1}H-^{15}N$-HSQC spectra of the ^{15}N-hPin1-WW (c(hPin1-WW) = 300 μM, 200 μL) titrated with CGSGGGpTPA (c(peptide) = 4 mM, total added volume 200 μL). The color coding corresponds to the total peptide concentration after consideration of dilution (**top**). Total signal shifts for the amino acids S16, Q33, W34, E35 plotted against the peptide concentration (**bottom**) and binding curves (solid lines) were fitted.

be assessed experimentally. Nevertheless, it is clear that each nanoparticle will be able to bind to more than one protein. This will be demonstrated in the following.

The interaction of the nanoparticles with the WW domain of hPin1 was analyzed by different techniques and compared with the dissolved peptides. Figure 13 shows the interaction of the

https://dx.doi.org/10.1021/acsabm.0c01424
ACS Appl. Bio Mater. 2021, 4, 945−965

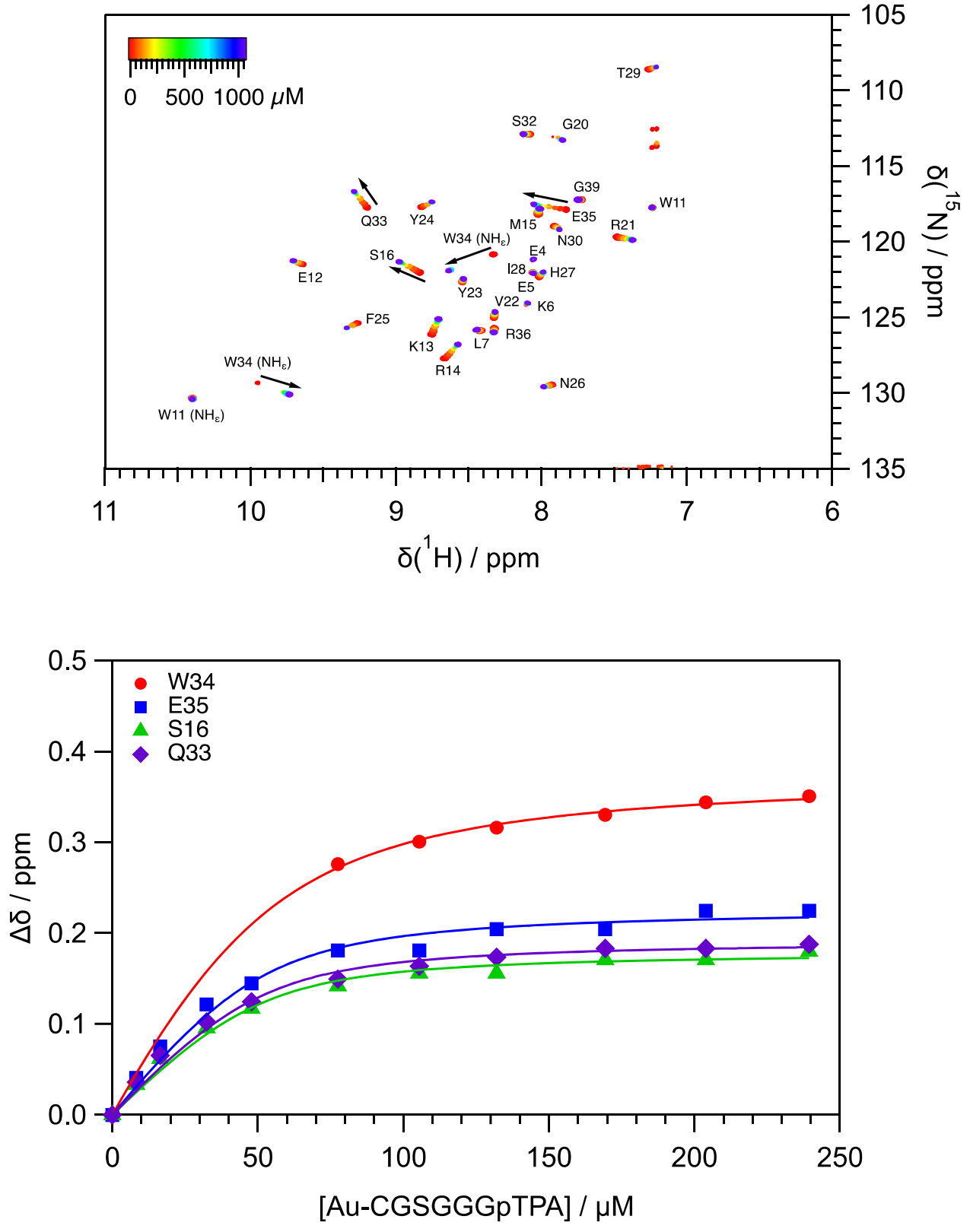

Figure 16. Overlay of $^{1}H-^{15}N$-HSQC spectra of the ^{15}N-WW-domain (c(hPin1-WW = 50 μM, 200 μL) titrated with Au-CGSGGGpTPA (c(AuNP) = 32.8 μM, c(peptide) = 4.9 mM, added volume at the end of the titration 55 μL) at pH 8 in potassium phosphate buffer. The color coding corresponds to the total peptide concentration after consideration of dilution (**top**). The total chemical shift perturbations for the amino acids S16, Q33, W34, and E35 were plotted against the effective peptide concentration which is the actual peptide concentration divided by 4.5 (see text) (**bottom**) and binding curves (solid lines) were fitted.

dissolved peptide CGGpTPA with ^{15}N-labeled hPin1-WW, measured by $^{1}H-^{15}N$-HSQC NMR titrations. The peptide was titrated stepwise to hPin1-WW until saturation occurred. A shift of the $^{1}H-^{15}N$ signals of the amino acids (S16, Q33,

https://dx.doi.org/10.1021/acsabm.0c01424
ACS Appl. Bio Mater. 2021, 4, 945−965

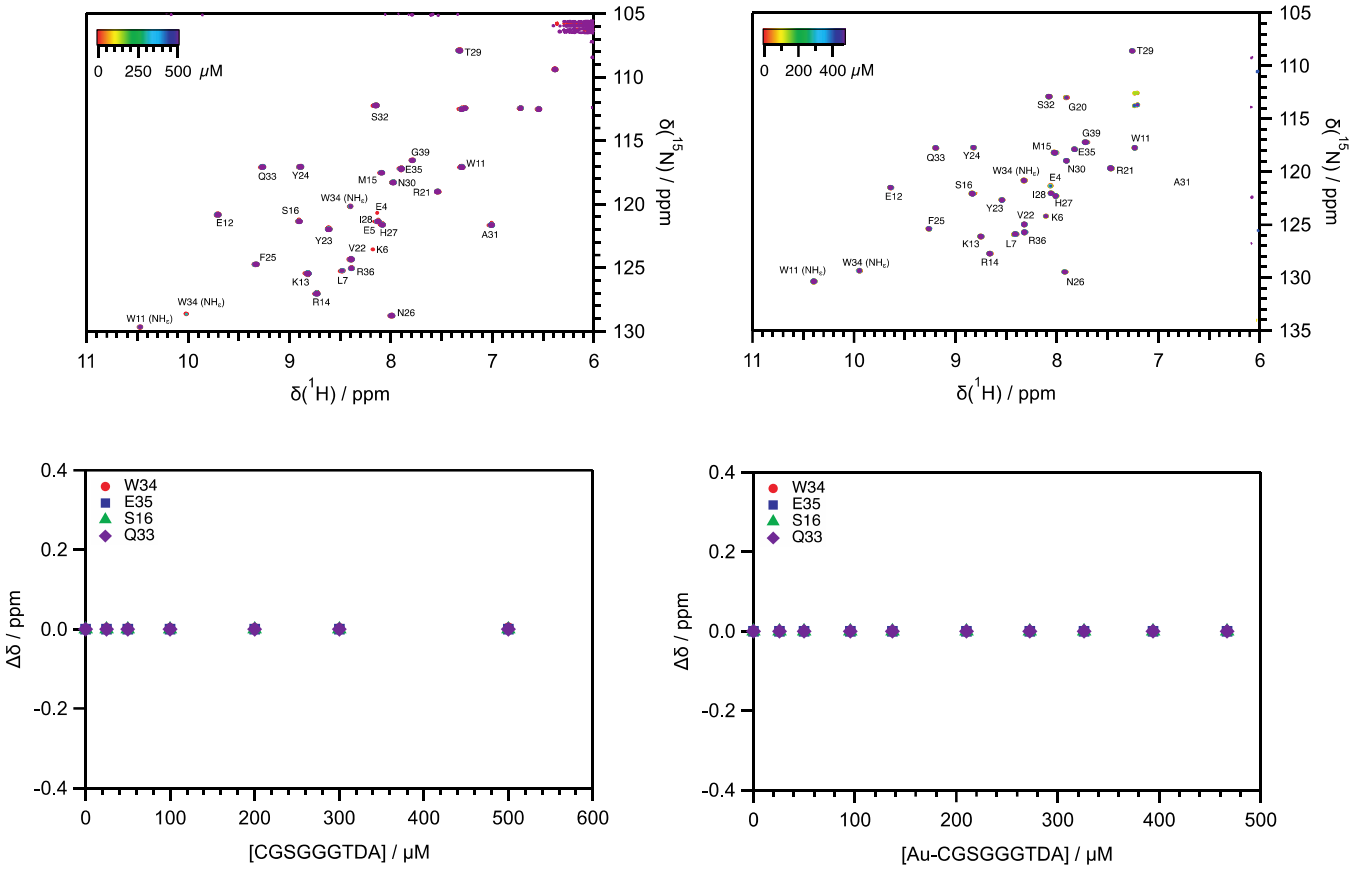

Figure 17. Overlay of $^{1}H-^{15}N$-HSQC spectra of the ^{15}N-WW-domain (c(hPin1-WW) = 50 μM, 200 μL) titrated with the nonbinding peptide CGSGGGTDA (c(peptide) = 1 mM, final added volume 200 μL) alone (**top left**) and conjugated to gold nanoparticles (c(AuNP) = 6.99 μM, c(CGSGGGTDA)=1.05 mM, final added volume 160 μL) (**top right**). The color coding corresponds to the total peptide concentration after consideration of dilution. Total chemical shift perturbations for the amino acids S16, Q33, W34, and E35 (**bottom left and right**) were plotted against the peptide end concentration (0.47 mM).

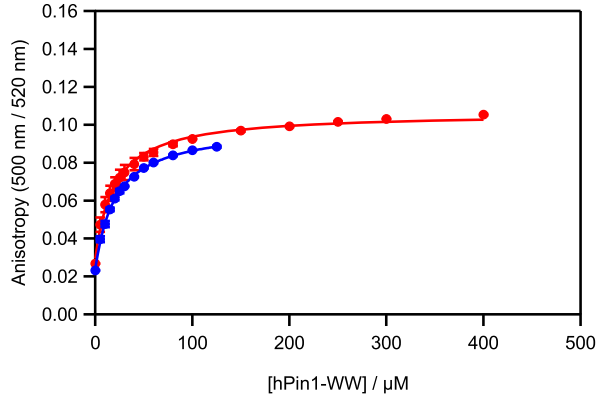

Figure 18. Binding between hPin1-WW (c(hPin1-WW) = 900 μM, finally added volume 48 μL) and Au-CGGpTPAAK(5,6-FAM)-NH_2 nanoparticles (c(AuNP) = 6.5 nM, c(peptide) = 0.9 μM; 60 μL) (**red**) and binding between hPin1-WW (c(hPin1-WW) = 300 μM, finally added volume 43 μL) and dissolved CGGpTPAAK(5,6-FAM)-NH_2 (c(peptide) = 0.1 μM, 60 μL) (**blue**). Each data point is the average of a triplicate measurement including the standard deviation.

W34, E35) that interact with the pT-P motif of the CGGpTPA was observed. A dissociation constant of K_D = 13 ± 3 μM was calculated by plotting the difference of the chemical shifts against the peptide concentration. This value is in good agreement with the dissociation constants for the binding of similar pT-P binding motif-containing peptides to hPin1-WW.[72]

Figure 14 shows the interaction of the CGGpTPA-conjugated nanoparticles with hPin1-WW. The gold nanoparticles were titrated stepwise to ^{15}N-labeled hPin1-WW up to saturation. We observed a significant change in the chemical shifts of the $^{1}H-^{15}N$ signals of amino acids (S16, Q33, W34, E35) that preferentially interact with the pTP motif of the peptide. The signal of tryptophan at position 34 disappeared due to the binding to the peptide on the gold nanoparticles and reappeared when the protein solution became saturated with nanoparticle-bound peptides. Notably, the nanoparticle-conjugated peptides interacted with the same amino acids as the free peptide. A dissociation constant of K_D = 308 ± 81 μM was calculated by plotting the difference of the chemical shifts of interest against the peptide concentration mM (calculated as 150 peptides per nanoparticle). Compared to the K_D of the unbound peptide, this value is significantly higher. This may indicate a weaker binding between nanoparticle-conjugated peptide and protein. On the other hand, it can also mean that there is an effective concentration of bound peptide which is well below the assumed concentration (150:1) shown above.

Assuming an equimolar one-site specific binding, the effective concentration and the K_D were calculated by assuming a similar dissociation constant as between dissolved peptide and protein, i.e. 13 μM. A 1:1 binding was still assumed, i.e. each peptide can bind to only one protein and vice versa.

https://dx.doi.org/10.1021/acsabm.0c01424
ACS Appl. Bio Mater. 2021, 4, 945−965

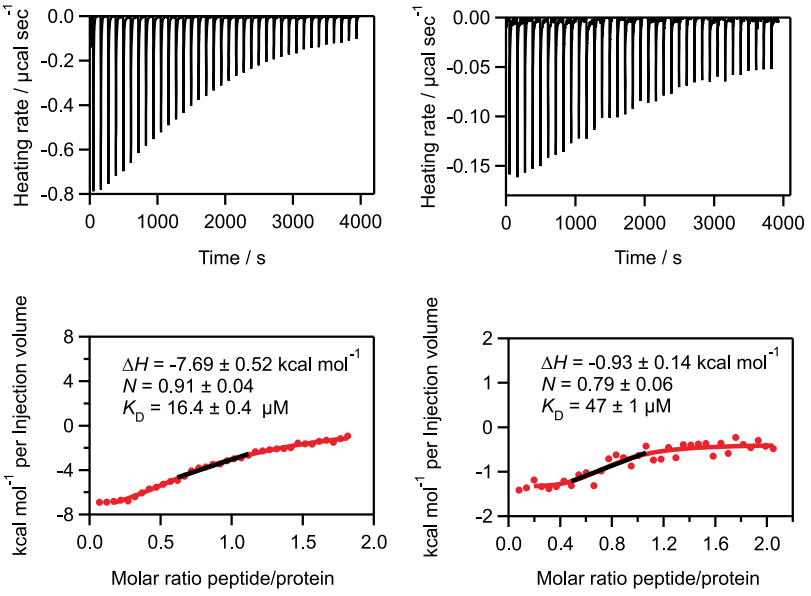

Figure 19. Enthalpy changes (**top**) and Wiseman plots (**bottom**) of CGGpTPA (c(peptide) = 1 mM, 36.4 μL) (**left**) and Au-CGGpTPA nanoparticles (c(AuNP) = 11.56 μM, c(peptide) = 1.74 mM, 150 peptide molecules per nanoparticle, finally added volume 36.4 μL) (**right**) during titration to hPin1-WW (c(hPin1-WW) = 100 μM, 300 μL). The curve fitting for the calculation of K_D was done with the Hill equation between points 2 and 35. The black line underlines the area of the point of inflection.

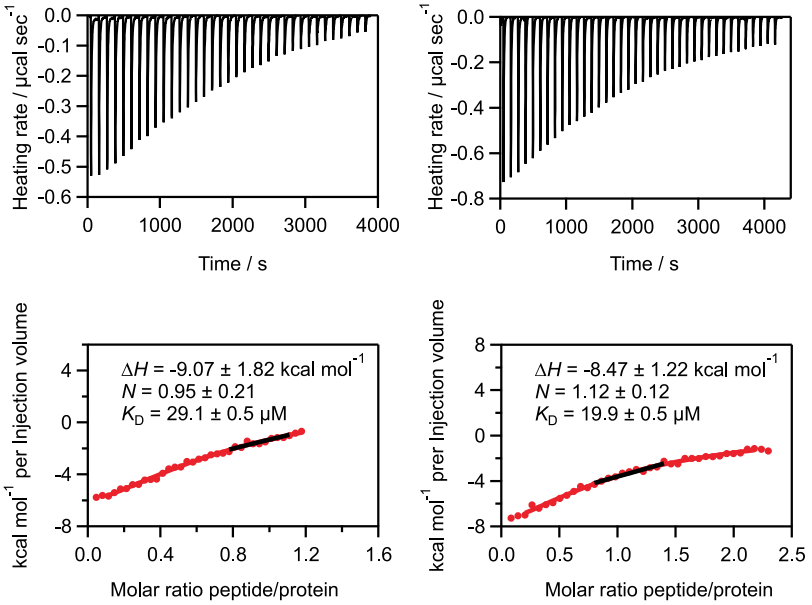

Figure 20. Enthalpy changes (**top**) and Wiseman plots (**bottom**) of CGSGGGpTPA peptide (c(peptide) = 1 mM, 36.4 μL) (**left**) and CGSGGGpTPA conjugated to gold nanoparticles (c(AuNP) = 12.03 μM, c(peptide) = 1.8 mM, finally added volume 36.4 μL) after titration to hPin1-WW (c(hPin1-WW) = 100 μM, 300 μL) (**right**). The curve fitting for the K_D calculation was done with the Hill equation between points 2 and 35. The black line underlines the range of the inflection point.

Then, the binding curve was approximated by letting the peptide concentration float, still using eq 4. This fit procedure gave a factor for the effective peptide concentration of 1:8.4 with a K_D of 12 ± 8 μM. In other words, out of 150 peptide molecules per nanoparticle, only 150/8.4 = 18 were actually binding to a protein. This is in very good agreement with the geometrically estimated number of protein molecules (i.e., 20) that can fit around one nanoparticle. Of course, there are a number of approximations in these considerations, but from a chemical and geometrical point of view, it makes sense that each nanoparticle is fully saturated on the surface with about 20 protein molecules at the end of the titration.

The peptide CGSGGGpTPA with three additional glycine units as spacer was investigated because it might enable a better binding of the pTP-motif to hPin1-WW due to steric reasons: If the peptide is too short to fully accommodate the width of one WW domain, the large gold core of the nanoparticle could sterically interfere with protein binding. For this peptide, we again observed a significant change in the chemical shift for the amino acids S16, Q33, W34, and E35 (Figure 15). A dissociation constant of 10 ± 1 μM was

https://dx.doi.org/10.1021/acsabm.0c01424
ACS Appl. Bio Mater. 2021, 4, 945−965

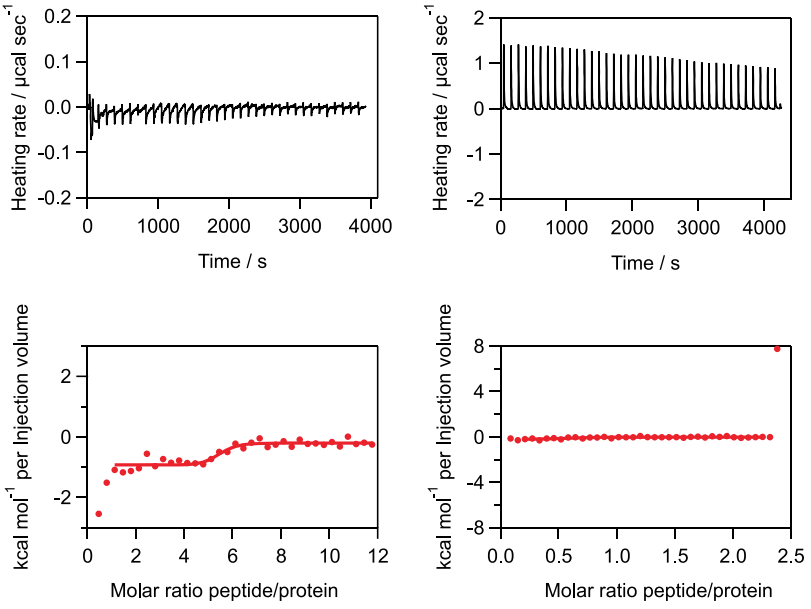

Figure 21. ITC titration curves of CGSGGGTDA peptide (c(peptide) = 1 mM, 36.4 μL) lacking the pTP recognition motif (**left**) titrated to hPin1-WW (c(hPin1-WW) = 10 μM, 300 μL) and Au-CGSGGGTDA nanoparticles (c(AuNP) = 6.22 μM, c(peptide) = 0.93 mM, 150 peptide molecules per nanoparticle, finally added volume 36.4 μL) titrated to hPin1-WW (c(hPin1-WW) = 50 μM, 300 μL) (**right**).

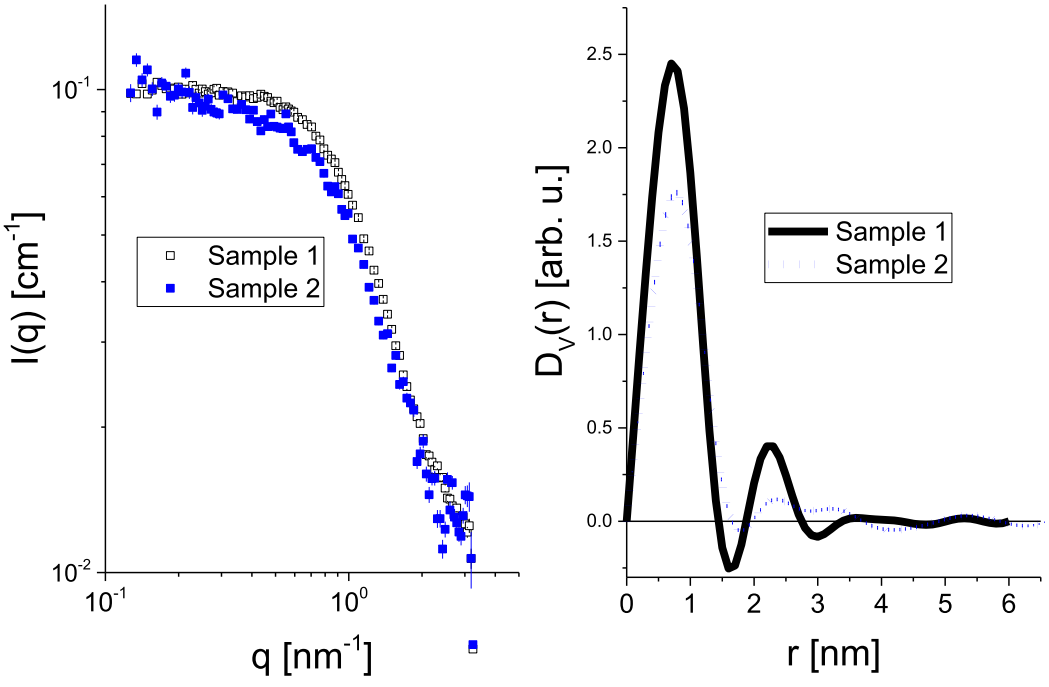

Figure 22. Small-angle X-ray scattering (SAXS) data of Au-CGSGGGpTPA nanoparticles in potassium phosphate buffer (**black curves**) and on Au-CGSGGGpTPA nanoparticles in the presence of 0.039 mM hPin1-WW in potassium phosphate buffer +10% D_2O (**blue curves**). (**left**) Primary SAXS data. (**right**) $D_V(r)$ function. The theoretical IFT-fits were omitted for clarity.

determined that is close to the dissociation constant of the peptide CGGpTPA (see above) and of comparable peptides.[72]

Figure 16 shows the interaction of CGSGGGpTPA-functionalized gold nanoparticles with hPin1-WW. Gold nanoparticles were titrated stepwise to ^{15}N-labeled hPin1-WW until saturation. A significant change in the chemical shift of the ^{1}H−^{15}N signals of the amino acids S16, Q33, W34, and E35 indicated the binding to hPin1-WW. Again, the signal of tryptophan at position 34 disappeared due to the binding of the conjugated peptide and reappeared when the WW domain solution became saturated with nanoparticle-conjugated peptides. A significantly higher K_D of 132 ± 4 μM was calculated assuming 150 peptides per nanoparticle.

The application of the same procedure as above led to a factor of the effective protein concentration of 1:4.5 and a K_D of 10 ± 4 μM. Thus, out of 150 peptides, only 150/4.5 = 33 are binding to proteins. This is more than with the shorter peptide CGGpTPA but reasonable because the spacer in the peptide increases the hydrodynamic radius of the nanoparticles from 4.4 to 5.4 nm. However, it is not sure whether this

https://dx.doi.org/10.1021/acsabm.0c01424
ACS Appl. Bio Mater. 2021, 4, 945−965

Table 2. K_D Values of Dissolved Peptides and Nanoparticle-Conjugated Peptides with the Protein hPin1-WW[a]

compound	method	K_D	binding model
CGGpTPA	NMR	13.3 ± 0.3 μM	1:1 binding
	ITC	16.4 ± 0.4 μM	1:1 binding
CGGpTAAK-(5,6)-FAM	FP	21 ± 1 μM	1:1 binding
Au-CGGpTPA	NMR	310 ± 80 μM	150 peptides per nanoparticle
Au-CGGpTPA	NMR	12 ± 8 μM	18 binding peptides per nanoparticle
	ITC	47 ± 1 μM	150 peptides per nanoparticle
Au-CGGpTAAK-(5,6)-FAM	FP	19 ± 1 μM	150 peptides per nanoparticle
CGGSGGGpTPA	NMR	10 ± 1 μM	1:1 binding
	ITC	29.1 ± 0.5 μM	1:1 binding
Au-CGGSGGGpTPA	NMR	132 ± 4 μM	150 peptides per nanoparticle
	NMR	10 ± 4 μM	33 binding peptides per nanoparticle
	ITC	19.9 ± 0.5 μM	150 peptides per nanoparticle
CGSGGGTDA	NMR	no binding	negative control
	ITC	no binding	negative control
Au-CGSGGGTDA	NMR	no binding	negative control
	ITC	no binding	negative control

[a]NMR = $^1H-^{15}N$-HSQC. ITC = isothermal titration calorimetry; FP = fluorescence polarization.

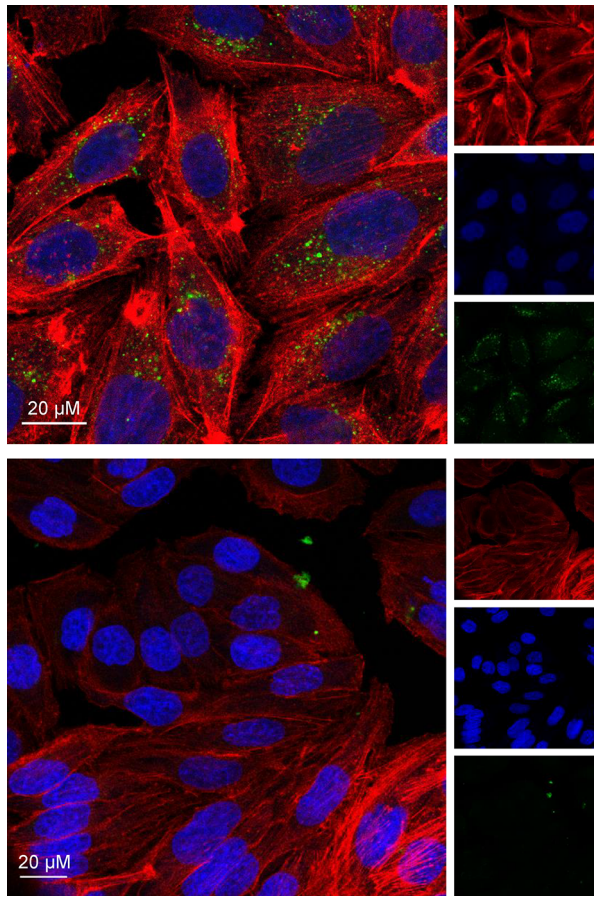

Figure 23. Confocal laser scanning microscopy images of HeLa cells (z-stacks across the cell), treated with green fluorescent Au-CGGpTPAAK-(5,6)-FAM nanoparticles (**top**) and CGGpTPAAK-(5,6)-FAM alone (control, **bottom**). Incubation time 24 h, nanoparticle concentration 12.5 μg mL^{-1}, 10^4 cells per well, 3.1 × 10^9 nanoparticles per well.

difference is significant in the light of the various assumptions made here. Tentatively, we can also conclude for these peptide-conjugated nanoparticles that the surface was fully covered after saturation with dissolved hPin1-WW protein.

To demonstrate that the interaction only occurs by the conjugated peptide and not to the gold nanoparticle core, the nonbinding control peptide CGSGGGTDA without the pTP motif was used. Figure 17 shows the $^1H-^{15}N$-HSQC spectra of free and nanoparticle-conjugated CGSGGGTDA in contact with hPin1-WW. No shift of signals occurred, i.e. no binding took place, as expected.

Fluorescence polarization (FP) is another powerful method to study the interaction between (fluorescent) peptides and proteins. Figure 18 compares the interaction of free CGGpTPAAK(5,6-FAM)-NH_2 peptide with hPin1-WW and of the peptide conjugated to gold nanoparticles with hPin1-WW, respectively. For unbound FAM-labeled peptide, a dissociation constant of 21 ± 1 μM was calculated, whereas the dissociation constant for the ligand conjugated to the gold nanoparticles was 19 ± 1 μM. These results are in a good agreement with the results from $^1H-^{15}N$-HSQC titration experiments.

Isothermal titration calorimetry (ITC) is probing the thermal effect of the peptide−protein interaction. Figure 19 shows the titration of either free CGGpTPA or Au-CGGpTPA to hPin1-WW. In both cases, an exothermal reaction was observed. By integrating the peaks and fitting the curve with the Hill equation, a dissociation constant of 16.4 ± 0.4 μM for the free peptide was determined with a molar binding stoichiometry of peptide to protein of 0.91 ± 0.04. This indicates a 1:1 binding of peptide to protein.

For the peptide conjugated to the gold nanoparticles, a higher dissociation constant of 47 ± 1 μM was determined, keeping the 1:1 binding model. The higher dissociation constant can be explained by the fact that, as shown above, not all peptides on the nanoparticle surface can bind to a protein. If we take 7.69 ± 0.52 kcal mol^{-1} as binding energy of one CGGpTPA to one hPin1-WW, we can estimate the number of binding peptides on the nanoparticles as follows: Each nanoparticle carries 150 peptides, and per peptide, we measured 0.93 kcal mol^{-1}. This gives a total interaction energy after saturation of 150 × (0.93 ± 0.14) = 140 ± 21 kcal mol^{-1}. If we divide this by the interaction energy of one peptide, we obtain (140 ± 21)/(7.69 ± 0.52) = 18 ± 4. Thus, about 18 peptides are binding which is again close to a total surface loading of 18 (by NMR) or 20 (by geometry) proteins on the surface of a nanoparticle after saturation.

Figure 20 shows the enthalpy changes of the longer CGSGGGpTPA peptide and of Au-CGSGGGpTPA nanoparticles after titration to hPin1-WW as measured by isothermal titration calorimetry. Again, exothermic reactions for free and bound peptide were observed. Dissociation constants of 29.1 ± 0.5 μM for the free peptide and of 19.9 ± 0.5 μM for Au-CGSGGGpTPA nanoparticles were computed, respectively. The binding energy per peptide on the nanoparticle was comparable to the binding energy of a dissolved peptide, probably due to the introduction of the spacer which facilitated the peptide−protein interaction.

https://dx.doi.org/10.1021/acsabm.0c01424
ACS Appl. Bio Mater. 2021, 4, 945−965

Figure 21 shows the enthalpy changes of the free control peptide CGSGGGTDA and of Au-CGSGGGTDA nanoparticles during titration to hPin1-WW. As expected, the enthalpy changes were small (in the range of the buffer control) Neither the peptide alone nor or conjugated to gold nanoparticles showed a significant binding affinity to the hPin1 WW domain.

The affinity data from NMR, FP, and ITC do not show whether a protein can cross-link two or more nanoparticles, e.g. by unspecific interactions. In principle, this is a possibility as each nanoparticle carries a number of protein-binding ligands. However, since each protein has only one peptide binding site, this is not likely but still possible. Therefore, we carried out SAXS experiments of nanoparticles after the addition of hPin1-WW. Figure 22 shows representative SAXS data. The results show a good dispersion and prove that the nanoparticles are not interconnected by the protein hPin1-WW as expected. However, as mentioned before in the text, the protein itself cannot be resolved due to the much weaker scattering power compared to the gold nanoparticle.

In Table 2, all values for the dissociation constants determined by different methods are summarized.

For most possible applications, intracellular protein targeting is of high interest. Therefore, we investigated whether peptide-conjugated ultrasmall nanoparticles are able to penetrate the cell wall in living cells. As reported earlier,[10,21] nanoparticles in the ultrasmall size range are capable to penetrate the cell membrane and may even enter the cell nucleus. Due to the fluorescent label, the peptide-functionalized gold nanoparticles can be traced inside the cells. Figure 23 shows the cellular uptake of FAM-labeled peptide-functionalized gold nanoparticles. By confocal laser scanning microscopy and z-stacks across the cell, a strong green fluorescence was located around the cell nucleus but not inside the nucleus. Beyond that, the exact intracellular localization of the nanoparticles was not studied here. In contrast to the nanoparticles, the fluorescent peptide alone did not penetrate the cell membrane. This in turn confirms that the peptide was firmly bound to the gold nanoparticles during cellular uptake.

It shall be noted that a ligand exchange of thiolated gold nanoparticles has been observed and quantitatively described.[69,73−79] In that case, one thiolated species is replacing another one. As this was not the case in our *in vitro* interaction studies between peptide-functionalized nanoparticles and the proteins due to the absence of other thiol-carrying ligands, it might occur in cell culture medium or inside a cell if thiolated proteins are present. However, the elucidation of this question must be left to future studies.

CONCLUSIONS

We have shown that a selective interaction between peptide-functionalized gold nanoparticles and a targeted protein is possible. With HRTEM, a nanoparticle core diameter of about 2 nm was observed, whereas the hydrodynamic diameter was about 5 nm (measured by ^{1}H-DOSY). The overall sizes and a stable dispersion of the gold nanoparticles were confirmed by SAXS experiments. The peptide concentration conjugated to the gold nanoparticle surface was obtained by quantitative NMR spectroscopy and by UV−vis spectroscopy, whereas the gold concentration was obtained by AAS. With this, we calculated a surface loading of about 150 peptides per gold nanoparticle (2 nm). NMR titration and ITC showed that about 20 peptides per nanoparticle can bind the protein hPin1-WW for the short peptide CGGpTPA. For the longer peptide CGSGGGpTPA, this number was 33. This was supported by geometric considerations of the size of a nanoparticle and the protein hPin1-WW. By NMR titration experiments, isothermal titration calorimetry, and fluorescence polarization spectroscopy, we determined dissociation constants for the dissolved peptides of 10−30 μM. Under the (unrealistic) assumption that all 150 peptides each bind to a protein, the K_D for such nanoparticles is considerably higher (100−300 μM) and probably wrong. However, if a reduced number of actually binding peptides is assumed, the dissociation constants are around 10−20 μM, i.e. comparable to the free peptides. This indicates that the attachment of the peptides to the gold nanoparticle surface does not change their function.

Enhanced binding of the nanoparticle-bound peptides due to a multi-activity effect is not observed because the protein exhibits only one peptide binding site. Hence, even though multiple peptides are present in close proximity, only one of them can be bound by each protein at the same time. When it comes to the recognition of a specific protein in a cell or a tissue, the situation of a complete nanoparticle surface saturation is unlikely because, in any biological medium, other proteins are present as well. Our control experiments with a nonbinding peptide clearly prove that no unspecific protein attachment to the nanoparticle surface occurs.

Cell uptake studies were performed with gold nanoparticles functionalized with a fluorescent binder peptide. The functionalized gold nanoparticles were able to penetrate the cell membrane whereas the peptide alone was not. This opens innovative opportunities for peptide-functionalized gold as nanocarriers for intracellular protein targeting.

ASSOCIATED CONTENT

Supporting Information

The Supporting Information is available free of charge at https://pubs.acs.org/doi/10.1021/acsabm.0c01424.

Additional DCS data, Stejskal−Tanner plots from ^{1}H NMR spectroscopy, and ^{1}H NMR spectra of dissolved peptides and peptide-conjugated gold nanoparticles (PDF)

AUTHOR INFORMATION

Corresponding Authors

Christine Beuck − *Department of Structural and Medicinal Biochemistry, Centre for Medical Biotechnology (ZMB), University of Duisburg-Essen, 45117 Essen, Germany*; Email: christine.beuck@uni-due.de

Matthias Epple − *Inorganic Chemistry and Center for Nanointegration Duisburg-Essen (CeNIDE), University of Duisburg-Essen, 45117 Essen, Germany*; orcid.org/0000-0002-1641-7068; Email: matthias.epple@uni-due.de

Authors

Tatjana Ruks − *Inorganic Chemistry and Center for Nanointegration Duisburg-Essen (CeNIDE), University of Duisburg-Essen, 45117 Essen, Germany*

Kateryna Loza − *Inorganic Chemistry and Center for Nanointegration Duisburg-Essen (CeNIDE), University of Duisburg-Essen, 45117 Essen, Germany*

Marc Heggen − *Ernst Ruska-Centre for Microscopy and Spectroscopy with Electrons, Forschungszentrum Jülich GmbH, 52425 Jülich, Germany*

https://dx.doi.org/10.1021/acsabm.0c01424
ACS Appl. Bio Mater. 2021, 4, 945−965

Oleg Prymak − *Inorganic Chemistry and Center for Nanointegration Duisburg-Essen (CeNIDE), University of Duisburg-Essen, 45117 Essen, Germany*

Andre Luiz Sehnem − *Institute of Physics, University of São Paulo, São Paulo 05508-090, Brazil;* orcid.org/0000-0002-3544-2277

Cristiano L. P. Oliveira − *Institute of Physics, University of São Paulo, São Paulo 05508-090, Brazil;* orcid.org/0000-0002-3426-6507

Peter Bayer − *Department of Structural and Medicinal Biochemistry, Centre for Medical Biotechnology (ZMB), University of Duisburg-Essen, 45117 Essen, Germany*

Complete contact information is available at: https://pubs.acs.org/10.1021/acsabm.0c01424

Notes

The authors declare no competing financial interest.

■ ACKNOWLEDGMENTS

The authors acknowledge financial support by the Deutsche Forschungsgemeinschaft (DFG) in the framework of the Collaborative Research Center SFB 1093: Supramolecular Chemistry on Proteins. We thank the Deutscher Akademischer Austauschdienst (DAAD, Germany) and the São Paulo Research Foundation (FAPESP grant 2019/06750-8) for support within a PPP exchange program. C.L.P.O. was supported by CAPES (grant 431/15), CNPq (grant 304861/2015-4), and the São Paulo Research Foundation (FAPESP, grants 2016/24531-3 and 2018/16092-5). A.L.S. was supported by the São Paulo Research Foundation (FAPESP, grant 2019/10433-8). This study was financed in part by the Coordenação de Aperfeiçoamento de Pessoal de Nível Superior, Brasil (CAPES, Finance Code 001). We thank Dr. Torsten Schaller and Dr. Felix Niemeyer for experimental assistance with NMR spectroscopy and Peter Binz for technical support. We thank Alma Rute for protein expression and purification. We thank Dr. Sebastian Kollenda for help with confocal laser scanning microscopy. We thank Kerstin Brauner and Robin Meya for elemental analyses. We thank Chantal Tekath for experimental assistance. We thank Prof. Hemmo Meyer for access to the ITC equipment. We thank Dr. Paulo R. A. F. Garcia and Dr. Arnaldo Gomes de Oliveira Filho for experimental assistance with SAXS experiments.

■ REFERENCES

(1) Vallet, C.; Aschmann, D.; Beuck, C.; Killa, M.; Meiners, A.; Mertel, M.; Ehlers, M.; Bayer, P.; Schmuck, C.; Giese, M.; Knauer, S. K. Functional disruption of the cancer-relevant interaction between survivin and histone H3 with a guanidiniocarbonyl pyrrole ligand. *Angew. Chem., Int. Ed.* **2020**, *59*, 5567−5571.

(2) van Dun, S.; Ottmann, C.; Milroy, L. G.; Brunsveld, L. Supramolecular chemistry targeting proteins. *J. Am. Chem. Soc.* **2017**, *139*, 13960−13968.

(3) Schrader, T.; Bitan, G.; Klärner, F. G. Molecular tweezers for lysine and arginine − powerful inhibitors of pathologic protein aggregation. *Chem. Commun.* **2016**, *52*, 11318−11334.

(4) Karim, A. A.; Dou, Q. Q.; Li, Z. B.; Loh, X. J. Emerging supramolecular therapeutic carriers based on host-guest interactions. *Chem. - Asian J.* **2016**, *11*, 1300−1321.

(5) Scaletti, F.; Hardie, J.; Lee, Y. W.; Luther, D. C.; Ray, M.; Rotello, V. M. Protein delivery into cells using inorganic nanoparticle-protein supramolecular assemblies. *Chem. Soc. Rev.* **2018**, *47*, 3421−3432.

(6) Kopp, M.; Kollenda, S.; Epple, M. Nanoparticle−protein interactions: Therapeutic approaches and supramolecular chemistry. *Acc. Chem. Res.* **2017**, *50*, 1383−1390.

(7) Rotello, V. M. Organic chemistry meets polymers, nanoscience, therapeutics and diagnostics. *Beilstein J. Org. Chem.* **2016**, *12*, 1638−1646.

(8) Tonga, G. Y.; Jeong, Y.; Duncan, B.; Mizuhara, T.; Mout, R.; Das, R.; Kim, S. T.; Yeh, Y. C.; Yan, B.; Hou, S.; Rotello, V. M. Supramolecular regulation of bioorthogonal catalysis in cells using nanoparticle-embedded transition metal catalysts. *Nat. Chem.* **2015**, *7*, 597−603.

(9) Sokolova, V.; Nzou, G.; van der Meer, S. B.; Ruks, T.; Heggen, M.; Loza, K.; Hagemann, N.; Murke, F.; Giebel, B.; Hermann, D. M.; Atala, A. J.; Epple, M. Ultrasmall gold nanoparticles (2 nm) can penetrate and enter cell nuclei in an in-vitro brain spheroid model. *Acta Biomater.* **2020**, *111*, 349−362.

(10) van der Meer, S. B.; Loza, K.; Wey, K.; Heggen, M.; Beuck, C.; Bayer, P.; Epple, M. Click chemistry on the surface of ultrasmall gold nanoparticles (2 nm) for covalent ligand attachment followed by NMR spectroscopy. *Langmuir* **2019**, *35*, 7191−7204.

(11) Ferreira, R. S.; Lira, A. L.; Torquato, R. J. S.; Schuck, P.; Sousa, A. A. Mechanistic insights into ultrasmall gold nanoparticle-protein interactions through measurement of binding kinetics. *J. Phys. Chem. C* **2019**, *123*, 28450−28459.

(12) Lira, A. L.; Ferreira, R. S.; Torquato, R. J. S.; Zhao, H.; Oliva, M. L. V.; Hassan, S. A.; Schuck, P.; Sousa, A. A. Binding kinetics of ultrasmall gold nanoparticles with proteins. *Nanoscale* **2018**, *10*, 3235−3244.

(13) Schmid, G.; Kreyling, W. G.; Simon, U. Toxic effects and biodistribution of ultrasmall gold nanoparticles. *Arch. Toxicol.* **2017**, *91*, 3011−3037.

(14) Lee, K. Y. J.; Lee, G. Y.; Lane, L. A.; Li, B.; Wang, J. Q.; Lu, Q.; Wang, Y. Q.; Nie, S. M. Functionalized, long-circulating, and ultrasmall gold nanocarriers for overcoming the barriers of low nanoparticle delivery efficiency and poor tumor penetration. *Bioconjugate Chem.* **2017**, *28* (1), 244−252.

(15) Boselli, L.; Polo, E.; Castagnola, V.; Dawson, K. A. Regimes of biomolecular ultrasmall nanoparticle interactions. *Angew. Chem., Int. Ed.* **2017**, *56*, 4215−4218.

(16) Zarschler, K.; Rocks, L.; Licciardello, N.; Boselli, L.; Polo, E.; Garcia, K. P.; De Cola, L.; Stephan, H.; Dawson, K. A. Ultrasmall inorganic nanoparticles: State-of-the-art and perspectives for biomedical applications. *Nanomedicine* **2016**, *12*, 1663−1701.

(17) Zhang, X.; Shastry, S.; Bradforth, S. E.; Nadeau, J. L. Nuclear uptake of ultrasmall gold-doxorubicin conjugates imaged by fluorescence lifetime imaging microscopy (FLIM) and electron microscopy. *Nanoscale* **2015**, *7*, 240−251.

(18) Zheng, K. Y.; Yuan, X.; Goswami, N.; Zhang, Q. B.; Xie, J. P. Recent advances in the synthesis, characterization, and biomedical applications of ultrasmall thiolated silver nanoclusters. *RSC Adv.* **2014**, *4*, 60581−60596.

(19) Luo, Z.; Zheng, K.; Xie, J. Engineering ultrasmall water-soluble gold and silver nanoclusters for biomedical applications. *Chem. Commun.* **2014**, *50*, 5143−5155.

(20) Kim, N. H.; Hackett, M. J.; Park, J.; Hyeon, T. Synthesis, characterization, and application of ultrasmall nanoparticles. *Chem. Mater.* **2014**, *26*, 59−71.

(21) Huo, S.; Jin, S.; Ma, X.; Xue, X.; Yang, K.; Kumar, A.; Wang, P. C.; Zhang, J.; Hu, Z.; Liang, X. J. Ultrasmall gold nanoparticles as carriers for nucleus-based gene therapy due to size-dependent nuclear entry. *ACS Nano* **2014**, *8*, 5852−5862.

(22) Leifert, A.; Pan-Bartnek, Y.; Simon, U.; Jahnen-Dechent, W. Molecularly stabilised ultrasmall gold nanoparticles: synthesis, characterization and bioactivity. *Nanoscale* **2013**, *5*, 6224−6242.

(23) Kwak, K.; Lee, D. Electrochemistry of atomically precise metal nanoclusters. *Acc. Chem. Res.* **2019**, *52*, 12−22.

(24) Zeng, C. J. Precision at the nanoscale: on the structure and property evolution of gold nanoclusters. *Pure Appl. Chem.* **2018**, *90*, 1409−1427.

(25) Sakthivel, N. A.; Dass, A. Aromatic thiolate-protected series of gold nanomolecules and a contrary structural trend in size evolution. *Acc. Chem. Res.* **2018**, *51*, 1774−1783.
(26) Jin, R. C.; Nobusada, K. Doping and alloying in atomically precise gold nanoparticles. *Nano Res.* **2014**, *7*, 285−300.
(27) Shang, L.; Dong, S. J.; Nienhaus, G. U. Ultra-small fluorescent metal nanoclusters: Synthesis and biological applications. *Nano Today* **2011**, *6*, 401−418.
(28) Kenzler, S.; Schrenk, C.; Frojd, A. R.; Hakkinen, H.; Clayborne, A. Z.; Schnepf, A. $Au_{70}S_{20}(PPh_3)_{12}$: an intermediate sized metalloid gold cluster stabilized by the Au_4S_4 ring motif and Au-PPh_3 groups. *Chem. Commun.* **2018**, *54*, 248−251.
(29) Du, X. S.; Jin, R. C. Atomic-precision engineering of metal nanoclusters. *Dalton Trans.* **2020**, *49*, 10701−10707.
(30) Häkkinen, H. The gold−sulfur interface at the nanoscale. *Nat. Chem.* **2012**, *4*, 443−455.
(31) Unal Gulsuner, H.; Ceylan, H.; Guler, M. O.; Tekinay, A. B. Multi-domain short peptide molecules for in situ synthesis and biofunctionalization of gold nanoparticles for integrin-targeted cell uptake. *ACS Appl. Mater. Interfaces* **2015**, *7*, 10677−10683.
(32) Nicol, J. R.; Dixon, D.; Coulter, J. A. Gold nanoparticle surface functionalization: a necessary requirement in the development of novel nanotherapeutics. *Nanomedicine* **2015**, *10*, 1315−1326.
(33) Paramelle, D.; Nieves, D.; Brun, B.; Kraut, R. S.; Fernig, D. G. Targeting cell membrane lipid rafts by stoichiometric functionalization of gold nanoparticles with a sphingolipid-binding domain peptide. *Adv. Healthcare Mater.* **2015**, *4*, 911−917.
(34) Bajaj, M.; Pandey, S. K.; Wangoo, N.; Sharma, R. K. Peptide functionalized metallic nanoconstructs: Synthesis, structural characterization, and antimicrobial evaluation. *ACS Biomater. Sci. Eng.* **2018**, *4*, 739−747.
(35) Monti, S.; Barcaro, G.; Sementa, L.; Carravetta, V.; Agren, H. Dynamics and self-assembly of bio-functionalized gold nanoparticles in solution: Reactive molecular dynamics simulations. *Nano Res.* **2018**, *11*, 1757−1767.
(36) Zhang, X. Y.; Wang, H.; Coulter, J. A.; Yang, R. J. Octaarginine-modified gold nanoparticles enhance the radiosensitivity of human colorectal cancer cell line LS180 to megavoltage radiation. *Int. J. Nanomed.* **2018**, *13*, 3541−3552.
(37) Cruz, E.; Kayser, V. Synthesis and enhanced cellular uptake in vitro of anti-HER2 multifunctional gold nanoparticles. *Cancers* **2019**, *11*, 870.
(38) Mahato, K.; Nagpal, S.; Shah, M. A.; Srivastava, A.; Maurya, P. K.; Roy, S.; Jaiswal, A.; Singh, R.; Chandra, P. Gold nanoparticle surface engineering strategies and their applications in biomedicine and diagnostics. *3 Biotechnol.* **2019**, *9*, 57.
(39) Sukumar, U. K.; Bose, R. J. C.; Malhotra, M.; Babikir, H. A.; Afjei, R.; Robinson, E.; Zeng, Y. T.; Chang, E.; Habte, F.; Sinclair, R.; Gambhir, S. S.; Massoud, T. F.; Paulmurugan, R. Intranasal delivery of targeted polyfunctional gold-iron oxide nanoparticles loaded with therapeutic microRNAs for combined theranostic multimodality imaging and presensitization of glioblastoma to Temozolomide. *Biomaterials* **2019**, *218*, 119342.
(40) Egorova, E. A.; van Rijt, M. M. J.; Sommerdijk, N.; Gooris, G. S.; Bouwstra, J. A.; Boyle, A. L.; Kros, A. One peptide for them all: Gold nanoparticles of different sizes are stabilized by a common peptide amphiphile. *ACS Nano* **2020**, *14*, 5874−5886.
(41) Ferreira, D.; Fontinha, D.; Martins, C.; Pires, D.; Fernandes, A. R.; Baptista, P. V. Gold nanoparticles for vectorization of nucleic acids for cancer therapeutics. *Molecules* **2020**, *25*, 3489.
(42) Riveros, A. L.; Eggeling, C.; Riquelme, S.; Adura, C.; Lopez-Iglesias, C.; Guzman, F.; Araya, E.; Almada, M.; Juarez, J.; Valdez, M. A.; Fuentevilla, I. A.; Lopez, O.; Kogan, M. J. Improving cell penetration of gold nanorods by using an amphipathic arginine rich peptide. *Int. J. Nanomed.* **2020**, *15*, 1837−1851.
(43) Salassa, G.; Burgi, T. NMR spectroscopy: a potent tool for studying monolayer-protected metal nanoclusters. *Nanoscale Horiz.* **2018**, *3*, 457.
(44) Guo, C.; Yarger, J. L. Characterizing gold nanoparticles by NMR spectroscopy. *Magn. Reson. Chem.* **2018**, *56*, 1074−1082.
(45) Schuetze, B.; Mayer, C.; Loza, K.; Gocyla, M.; Heggen, M.; Epple, M. Conjugation of thiol-terminated molecules to ultrasmall 2 nm-gold nanoparticles leads to remarkably complex 1H-NMR spectra. *J. Mater. Chem. B* **2016**, *4*, 2179−2189.
(46) Hogeweg, A.; Sowislok, A.; Schrader, T.; Beuck, C. An NMR method to pinpoint supramolecular ligand binding to basic residues on proteins. *Angew. Chem., Int. Ed.* **2017**, *56*, 14758−14762.
(47) Macias, M. J.; Hyvonen, M.; Baraldi, E.; Schultz, J.; Sudol, M.; Saraste, M.; Oschkinat, H. Structure of the WW domain of a kinase-associated protein complexed with a proline-rich peptide. *Nature* **1996**, *382* (6592), 646−9.
(48) Wintjens, R.; Wieruszeski, J. M.; Drobecq, H.; Rousselot-Pailley, P.; Buée, L.; Lippens, G.; Landrieu, I. 1H NMR study on the binding of Pin1 Trp-Trp domain with phosphothreonine peptides. *J. Biol. Chem.* **2001**, *276*, 25150−25156.
(49) Lu, P. J.; Zhou, X. Z.; Shen, M.; Lu, K. P. Function of WW domains as phosphoserine- or phosphothreonine-binding modules. *Science* **1999**, *283* (5406), 1325−8.
(50) Poole, L. B. The basics of thiols and cysteines in redox biology and chemistry. *Free Radical Biol. Med.* **2015**, *80*, 148−157.
(51) Tam, J. P.; Wu, C. R.; Liu, W.; Zhang, J. W. Disulfide bond formation in peptides by dimethyl sulfoxide. Scope and applications. *J. Am. Chem. Soc.* **1991**, *113*, 6657−6662.
(52) Thust, A.; Barthel, J.; Tillmann, K. FEI Titan 80−300 TEM. *J. Large-Scale Res. Fac.* **2016**, *2*, A41.
(53) Altieri, A. S.; Hinton, D. P.; Byrd, R. A. Association of biomolecular systems via pulsed-field gradient NMR self-diffusion measurements. *J. Am. Chem. Soc.* **1995**, *117*, 7566−7567.
(54) Stejskal, E. O.; Tanner, J. E. Spin diffusion measurements: Spin echoes in the presence of a time-dependent field gradient. *J. Chem. Phys.* **1965**, *42*, 288.
(55) Akoka, S.; Barantin, L.; Trierweiler, M. Concentration measurement by proton NMR using the ERETIC method. *Anal. Chem.* **1999**, *71*, 2554−2557.
(56) Ayed, A.; Mulder, F. A.; Yi, G. S.; Lu, Y.; Kay, L. E.; Arrowsmith, C. H. Latent and active p53 are identical in conformation. *Nat. Struct. Biol.* **2001**, *8*, 756−760.
(57) Williamson, M. P. Using chemical shift perturbation to characterise ligand binding. *Prog. Nucl. Magn. Reson. Spectrosc.* **2013**, *73*, 1−16.
(58) Wiseman, T.; Williston, S.; Brandts, J. F.; Lin, L. N. Rapid measurement of binding constants and heats of binding using a new titration calorimeter. *Anal. Biochem.* **1989**, *179*, 131−137.
(59) Hammersley, A. P.; Svensson, S. O.; Hanfland, M.; Fitch, A. N.; Hausermann, D. Two-dimensional detector software: From real detector to idealised image or two-theta scan. *High Pressure Res.* **1996**, *14*, 235−248.
(60) Oliveira, C. L. P. Investigating macromolecular complexes in solution by small angle x-ray scattering. In *Current Trends in X-Ray Crystallography*; Chandrasekaran, D. A., Ed.; InTech: 2011; pp 367−392.
(61) Garcia, P. R. A. F.; Loza, K.; Daumann, S.; Grasmik, V.; Pappert, K.; Rostek, A.; Helmlinger, J.; Prymak, O.; Heggen, M.; Epple, M.; Oliveira, C. L. P. Combining small-angle x-ray scattering and x-ray powder diffraction to investigate size, shape and crystallinity of silver, gold and alloyed silver-gold nanoparticles. *Braz. J. Phys.* **2019**, *49* (2), 183−190.
(62) Oliveira, C. L. P.; Behrens, M. A.; Pedersen, J. S.; Erlacher, K.; Otzen, D.; Pedersen, J. S. A SAXS study of glucagon fibrillation. *J. Mol. Biol.* **2009**, *387*, 147−161.
(63) Luh, L. M.; Hansel, R.; Lohr, F.; Kirchner, D. K.; Krauskopf, K.; Pitzius, S.; Schafer, B.; Tufar, P.; Corbeski, I.; Guntert, P.; Dotsch, V. Molecular crowding drives active Pin1 into nonspecific complexes with endogenous proteins prior to substrate recognition. *J. Am. Chem. Soc.* **2013**, *135*, 13796−13803.
(64) Svergun, D.; Barberato, C.; Koch, M. H. J. CRYSOL− a program to evaluate X-ray solution scattering of biological macro-

https://dx.doi.org/10.1021/acsabm.0c01424
ACS Appl. Bio Mater. 2021, 4, 945−965

molecules from atomic coordinates. *J. Appl. Crystallogr.* **1995**, *28*, 768−773.
(65) Oliveira, C. L. P.; Juul, S.; Jorgensen, H. L.; Knudsen, B.; Tordrup, D.; Oteri, F.; Falconi, M.; Koch, J.; Desideri, A.; Pedersen, J. S.; Andersen, F. F.; Knudsen, B. R. Structure of nanoscale truncated octahedral DNA cages: Variation of single-stranded linker regions and influence on assembly yields. *ACS Nano* **2010**, *4*, 1367−1376.
(66) Semenyuk, A. V.; Svergun, D. I. GNOM− a program package for small-angle scattering data processing. *J. Appl. Crystallogr.* **1991**, *24*, 537−540.
(67) Mahl, D.; Diendorf, J.; Meyer-Zaika, W.; Epple, M. Possibilities and limitations of different analytical methods for the size determination of a bimodal dispersion of metallic nanoparticles. *Colloids Surf., A* **2011**, *377*, 386−392.
(68) Ruks, T.; Beuck, C.; Schaller, T.; Niemeyer, F.; Zähres, M.; Loza, K.; Heggen, M.; Hagemann, U.; Mayer, C.; Bayer, P.; Epple, M. Solution NMR spectroscopy with isotope-labelled cysteine (^{13}C, ^{15}N) reveals the surface structure of L-cysteine-coated ultrasmall gold nanoparticles (1.8 nm). *Langmuir* **2019**, *35*, 767−778.
(69) Smith, A. M.; Marbella, L. E.; Johnston, K. A.; Hartmann, M. J.; Crawford, S. E.; Kozycz, L. M.; Seferos, D. S.; Millstone, J. E. Quantitative analysis of thiolated ligand exchange on gold nanoparticles monitored by ^{1}H NMR spectroscopy. *Anal. Chem.* **2015**, *87*, 2771−2778.
(70) van der Meer, S. B.; Seiler, T.; Buchmann, C.; Partalidou, G.; Boden, S.; Loza, K.; Heggen, M.; Linders, J.; Prymak, O.; Oliveira, C. L. P.; Hartmann, L.; Epple, M. Controlling the surface functionalization of ultrasmall gold nanoparticles by sequence-defined macromolecules. *Chem. - Eur. J.* **2020**, DOI: 10.1002/chem.202003804.
(71) Ruks, T.; Loza, K.; Heggen, M.; Ottmann, C.; Bayer, P.; Beuck, C.; Epple, M. Targeting the surface of the protein 14−3-3 by ultrasmall gold nanoparticles (1.5 nm), carrying the specific peptide CRaf. *ChemBioChem* **2020**, DOI: 10.1002/cbic.202000761.
(72) Verdecia, M. A.; Bowman, M. E.; Lu, K. P.; Hunter, T.; Noel, J. P. Structural basis for phosphoserine-proline recognition by group IV WW domains. *Nat. Struct. Biol.* **2000**, *7*, 639−643.
(73) Zan, X. F.; Li, Q. Z.; Pan, Y. T.; Morris, D. J.; Zhang, P.; Li, P.; Yu, H. Z.; Zhu, M. Z. Versatile ligand-exchange method for the synthesis of water-soluble monodisperse AuAg nanoclusters for cancer therapy. *ACS Appl. Nano Mater.* **2018**, *1*, 6773−6781.
(74) Dinkel, R.; Peukert, W.; Braunschweig, B. In situ spectroscopy of ligand exchange reactions at the surface of colloidal gold and silver nanoparticles. *J. Phys.: Condens. Matter* **2017**, *29*, 133002.
(75) Zhang, Z.; Xu, L.; Li, H.; Kong, J. Wavelength-tunable luminescent gold nanoparticles generated by cooperation ligand exchange and their potential application in cellular imaging. *RSC Adv.* **2013**, *3*, 59−63.
(76) Heinecke, C. L.; Ni, T. W.; Malola, S.; Mäkinen, V.; Wong, O. A.; Häkkinen, H.; Ackerson, C. J. Structural and theoretical basis for ligand exchange on thiolate monolayer protected gold nanoclusters. *J. Am. Chem. Soc.* **2012**, *134*, 13316−13322.
(77) Reyes, E.; Madueño, R.; Blázquez, M.; Pineda, T. Facile exchange of ligands on the 6-mercaptopurine-monolayer protected gold clusters surface. *J. Phys. Chem. C* **2010**, *114*, 15955−15962.
(78) Hong, R.; Fernandez, J. M.; Nakade, H.; Arvizo, R.; Emrick, T.; Rotello, V. M. In situ observation of place exchange reactions of gold nanoparticles. Correlation of monolayer structure and stability. *Chem. Commun.* **2006**, 2347−2349.
(79) Hostetler, M. J.; Templeton, A. C.; Murray, R. W. Dynamics of place-exchange reactions on monolayer-protected gold cluster molecules. *Langmuir* **1999**, *15*, 3782−3789.

https://dx.doi.org/10.1021/acsabm.0c01424
ACS Appl. Bio Mater. 2021, 4, 945−965